IPP-Report

IPP Max-Planck-Institut für Plasmaphysik

H.-S. Bosch, P. Franzen, O. Gruber, S. Günter
B. Heinemann, M. Kaufmann, K. Lackner,
J. Neuhauser, G. Pereverzev, R. Riedl, C. Sihler,
E. Speth, A. Stäbler, B. Streibl, O. Vollmer, R. Wolf

Extension of the ASDEX Upgrade Programme: Tangential Neutral Beam Injection (TNBI) and Reactive Power Compensation (RPC) Application for Preferential Support, Phase I und II

IPP 1/318
Dezember 1998

Extension of the ASDEX Upgrade Programme: Tangential Neutral Beam Injection (TNBI) and Reactive Power Compensation (RPC) Application for Preferential Support, Phase I and II

H.-S. Bosch, P. Franzen, O. Gruber, S. Günter
B. Heinemann, M. Kaufmann, K. Lackner,
J. Neuhauser, G. Pereverzev, R. Riedl, C. Sihler,
E. Speth, A. Stäbler, B. Streibl, O. Vollmer, R. Wolf

22 December 1998

Abstract

This report contains the combined application for preferential support for Tangential Neutral Beam Injection (TNBI) and Reactive Power Compensation (RPC) for ASDEX Upgrade to EURATOM. Only the sections concerning the projected costs and manpower requirements were omitted in this report.

The application, which comprised both phases of the approval procedure (i.e. phase I and phase II), was submitted to the CCFP in February of 1998 (EUR FU (98) CCFP 75/8.1). On March 30/31, the AdHoc group visited IPP to evaluate the proposal. On June 19, 1998 the project was approved by the CCFP.

Contents

1 EXECUTIVE SUMMARY

During the next few years ASDEX Upgrade will strengthen its efforts concerning investigations of advanced tokamak scenarios in connection with divertor operation. Such operating modes have been recognized as the most promising option for an economically attractive tokamak reactor, and they play already an important role for the ITER operating scenarios.

This requires a current drive capability of about 250 kA, which – together with a bootstrap current fraction of 70% – will allow quasistationary advanced tokamak operation at a plasma current of 1 MA.

- In this regime, enhanced beta and confinement may be achieved by a flat/reversed magnetic shear profile in the plasma center, requiring the toroidal plasma current profile to peak near half radius (r/a = 0.5).
- To fully exploit these capabilities, a flattop time of at least 2-3 skin times, i.e., 10 seconds is necessary.

The modifications following from these two basic requirements are the topic of this preferential support application, which is submitted both for phase I and phase II approval, because the phase II aspects of the proposal are intrinsically linked to the phase I issues. Furthermore, the divertor was redesigned into a shape similar to the actual ITER divertor. The lyra-shaped divertor II has been in operation since May 1997 and has produced very important results in the meantime.

1.1 Tangential NBI

One main option to drive about 250 kA off-axis plasma current in ASDEX Upgrade is tangential off-axis neutral beam injection. There is a particular way by which neutral beam injection will achieve deposition at half radius and simultaneously maintain sufficiently high parallel velocity: choosing an enhanced angle of inclination of the injected beams with respect to the horizontal midplane causes the beams to travel significantly above and below the midplane when reaching the radius of tangency. The power deposition and current density profiles achieved with this geometry are remarkably invariant with respect to changes of plasma density and radial as well as vertical plasma position. Numerical simulation shows that about 5 MW of 100 keV D^0 will be sufficient for 250 kA to be driven. This corresponds to the power injected by two PINIs aiming at a radius of tangency of $R_T = 1.29\,\mathrm{m}$ ($= 0.78\,R_0$) under angles of inclination of $\pm\ 6.7^0$ with respect to the midplane.

Rather than adding a third injector, it is proposed to modify the second injector, which is suited for 100 keV. The necessary modifications include:

(i) a movement of the injector as a whole into a more tangential orientation with a slight increase of the distance from the porthole; this necessitates modifications on the ASDEX Upgrade injector port and the structure;

(ii) an internal redesign of the injector components in order to achieve a higher angle of inclination (from presently $\pm$ 4.9^0 to then $\pm$ 6.7^0) for the more tangential pair of beams, leaving the more radial pair of beams unchanged.

1.2 Reactive Power Compensation

ASDEX Upgrade long puls operation of 10 s will be achieved by a reduction of the plasma current to a value of $I_p = 1$ MA.

In contrast to the short puls operation (e.g. 4-5 s at 1.4 MA), it is required for the 1 MA long puls operation to fully exploit the fly wheel energy of the two poloidal field (PF) generators EZ3[1] and EZ4[2]. Unfortunately the less powerful EZ3 generator provides in relation to the EZ4 generator a 40% larger ratio of fly wheel energy to apparent power. This means, that compared to short pulse operation without energy constraint, the load sharing ratio EZ3/EZ4 has to be increased for long pulse operation in order to be able to synchronously and thus completely unload both fly wheels. This obvious contradiction can only be resolved by extensive reactive power compensation for the EZ3 generator.

Satisfactory conditions for long pulse operation can be achieve with a reactive power compensation plant of 120 MVAr (referred to a frequency of 100 Hz). As a power compensation of about 30 MVAr already has proven to be necessary for 5 s pulses at high plasma currents ($\geq$ 1.4 MA) and full heating power, a pilot capacitor module with 30 MVAr has already been ordered in late 1997, which will be paid fully by the IPP budget without preferential support by EURATOM. This module is also intended to provide the technical basis for defining the exact requirements of the further 3 modules with a total rating of 90 MVAr, which are the subject of this preferential support application. Included are the efforts for civil engineering, buildings, bus work and generator voltage protection.

It should be stated that this extension of the power supply systems is necessary only for the ASDEX Upgrade long pulse (10 s) operations and is not needed for any other use in IPP.

[1] (EZ3: 500 MJ in principle useable flywheel energy, 144 MVA short pulse apparent power)
[2] (EZ4: 650 MJ in principle useable flywheel energy, 260 MVA short pulse apparent power)

2 INTRODUCTION

Designed in the period of 1980-1984, ASDEX Upgrade, with its elliptical cross section and its poloidal divertor, forms, together with JET, COMPASS and other experiments, an essential basis for the preparation of and the extrapolation to ITER. To adapt ASDEX Upgrade to the scientific progress and to strengthen its flexibility, the original heating of 6 MW ICRH and 10 MW NBI (deuterium 60 keV) was expanded further by 10 MW of NBI with the option of a beam energy of 100 keV and 2 MW of ECRH (partly in operation, partly under construction).

It is now proposed to enhance the reactor relevance of ASDEX Upgrade by two further modification in order to exploit the potential of the device. It is being proposed on the one hand to redirect two beams out of the 100 kV NBI system into a more tangential direction to allow for current drive. At the same time it is proposed to add a reactive power compensation system, to allow for a full use of the existing fly-wheel generators and a consequent extension of the operating envelope of ASDEX Upgrade in pulse length and/or magnetic field and current.

Both applications for preferential support are jointly described in this proposal because they are based on a common physics ground. Both applications ask for phase I and II examination because the applicants believe that with respect to the NBI part the phase II aspects of the proposal are intrinsically linked to the phase I issues and that is even more so the case for the reactive power compensation. Furthermore, the technical design is sufficiently well developed so that all pertinent features can already be adequately presented now.

In the following the main features and parameters of ASDEX Upgrade are summarized, and then the basic aims and the achievements described (chapter 3). Based on this the aims of ASDEX Upgrade which could be pursued with the proposed actions are outlined in chapter 4. Chapter 5 discusses in more detail the physics motivation for off-axis current drive by **T**angential **N**eutral **B**eam **I**njection (TNBI) and for 10 second pulse length operation, requiring **R**eactive **P**ower **C**ompensation (RPC). The technical concept and design for TNBI is described in chapter 6 and for RPC in chapter 7.

3 ASDEX UPGRADE: PARAMETERS, TARGETS AND ACHIEVEMENTS

3.1 Parameters of ASDEX Upgrade

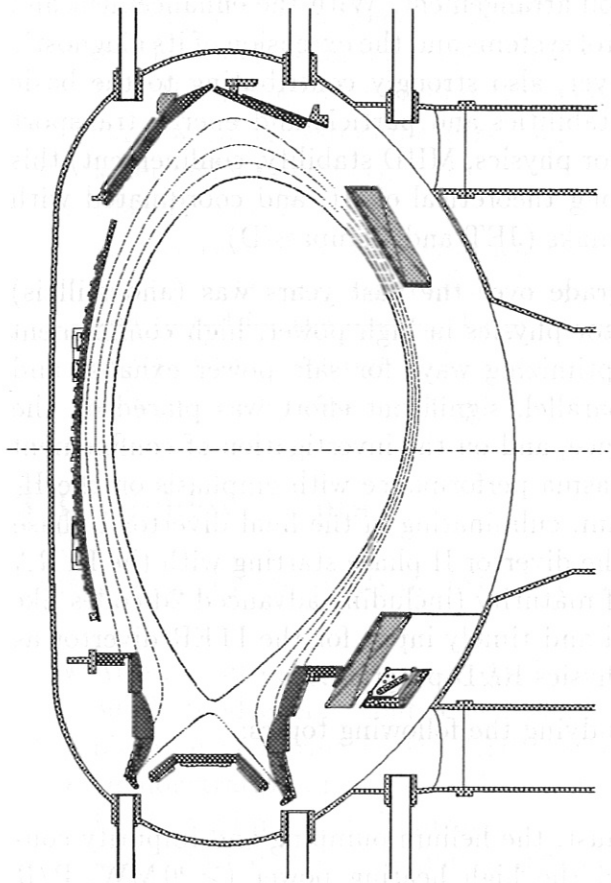

Figure 1: ASDEX Upgrade cross-section. ASDEX Upgrade is an elliptical cross-section tokamak with an ITER-type poloidal divertor.

The essential device parameters of ASDEX Upgrade are:

plasma current	$I_p \leq 1.6$ MA
magnetic field	$B_t \leq 3.1$ T
major radius	$R_o = 1.65$ m
minor radius	a = 0.5 m
ellipticity	$\kappa \leq 1.8$
triangularity	$\delta_{top} \leq 0.1$; $\delta_{bottom} \leq 0.3$ (δ_{top}, $\delta_{bottom} \leq 0.4$ in fall of 1998)
single-null divertor (double-null possible)	
neutral beam injection	$U = 65/100$ keV, $P_{NBI} = 20$ MW (for D_2)
ICRH	$\nu = 30 \ldots 120$ MHz, $P_{ICRH} \leq 6$ MW
ECRH	$\nu = 140$ GHz, $P_{ECRH} = 2$ MW (partly operational)
pumping	14 turbomolecular pumps: $S_{D_2} = 10$ m^3 s^{-1} in pump chamber; cryopump: $S_{D_2} = 100$ m^3 s^{-1}

Target plates and near-plasma surfaces are covered with graphite (CFC at target tiles), and all surfaces are generally boronized.

3.2 Scientific Aims

The primary design aim of the ASDEX Upgrade divertor tokamak was to realize a reactor-compatible divertor and study reactor-relevant plasma edge physics. Experiments on ASDEX Upgrade have therefore always been strongly focused on the critical R&D tasks for ITER. Originally, this implied mainly studies of divertor behavior and control issues relating to its ITER-like configuration and coil arrangement. With the enhancement and diversification of its heating and particle control systems and the extension of its diagnostic capabilities, ASDEX Upgrade is now, however, also strongly contributing to the basic understanding of magnetohydrodynamic instabilities and particle and energy transport in the bulk plasma. In all three areas (divertor physics, MHD stability, confinement) this experimental work is accompanied by a strong theoretical effort, and coordinated with studies on the other European divertor tokamaks (JET and Compass-D).

The experimental program of ASDEX Upgrade over the past years was (and still is) focused to a large extent on edge and divertor physics in high power, high confinement regimes, with the aim of identifying and optimizing ways for safe power exhaust and particle control for next step devices. In parallel, significant effort was placed on the investigation of disruptions and their avoidance, and on the investigation of confinement scaling and on the improvement of global plasma performance with emphasis on the H-mode. The edge and divertor physics program, culminating in the final divertor I phase with tungsten target plates in 1995/96 and the divertor II phase starting with the LYRA configuration in 1997, has reached a status of maturity (including advanced 2d-codes like B2-EIRENE), which is providing the desired and timely input for the ITER divertor as an integral part of the international ITER physics R&D program.

At present, ASDEX Upgrade is especially studying the following topics:

- Exhaust physics
  Search for solutions for the power exhaust, the helium pumping and impurity control. In connection with the divertor, the high heating power (≥ 20 MW, P/R ≥ 12 MW/m) is especially important for relevant studies.
- Refuelling
  In addition to conventional gas puffing systems in the main and divertor chamber, ASDEX Upgrade is using quasi-stationary, feedback-controlled refuelling by pellets launched from both the low and high field side of the plasma, which demonstrates large improvement in fuelling efficiency in the latter case. Density control in both scenarios is made possible by the simultaneous availability of a powerful pumping system.
- H-mode physics
  A solution for good power and particle exhaust must be compatible with good confinement, and consequently, with good H-mode performance. Further investigation of H-mode physics is necessary to extend the H-mode operation regime to favourable high edge densities.
- Confinement studies
  Due to its ITER-like shape, ASDEX Upgrade can contribute relevant data to the general confinement data base and to dimensionless scaling studies. In particular, however, its powerful heating, fuelling and pumping systems and its extensive set of edge diagnostics allow the illumination of the connection between edge parameters

and core confinement and the clarification of the physics processes arising close to regime and operating limits (L/H-transition, density limit with gas puff and with pellet refuelling).

- MHD investigation
  MHD phenomena have been found to play a part not only in operating limits, but also in quasi-steady state conditions, affecting energy confinement and sometimes leading to bifurcations in operating space. ASDEX Upgrade studies in particular ELMs, neoclassical modes (including the possibility of feedback control by localized ECRH heating and current drive), and fast particle induced modes, and builds up an early warning system for disruptions and a disruption mitigation system (including killer pellet injection).
- Plasma control
  As a consequence of the elliptical cross-section ($\kappa \approx 1.6$), the position of the plasma has to be actively controlled. In addition, control scenarios have to be developed and tested for the plasma shape, other plasma parameters and ramp-up and ramp-down of the discharge. The disruptions in elliptical cross-section plasmas are also being studied (forces, energy deposition, halo currents).

3.3 Achievements

Outstanding physics results of ASDEX Upgrade in the recent past were:

- Attainment of quasistationary H-mode with large radiated power fraction (up to 80%), good energy confinement, and negligible power loads on the divertor target plates, even during ELMs (CDH-mode).
- Demonstration of helium exhaust, in H-mode plasmas significantly exceeding the ITER minimum requirements.
- Quantitative understanding of critical divertor properties (e.g., pumping capability for different gaseous impurities, role of volume recombination in divertor detachment) through a combined measurement and modelling effort.
- Successful operation with tungsten-coated divertor target plates, resulting - under high-power operating conditions - in well tolerable core tungsten concentrations.
- Characterization of different edge operating conditions (L-mode, type-I and type-III ELMs) through measurement of the local edge parameters, in particular T_e and n_e. Introduction of a now universally used parametric representation ("ASDEX Upgrade diagram"), illuminating also the role of the ballooning and the density limit. This work was also accompanied by significant progress in the clarification of the connection between core transport and edge behavior.
- Clarification of the different nature of density limit phenomena in L- and H-mode plasmas.
- Demonstration that pellet injection from the high-field side can overcome the problem of poor fuelling efficiency encountered in high-power H-mode discharges with conventional pellet refuelling from the low field side (this extension on the fuelling system had been prompted by a theoretical explanation of the poorer fuelling efficiency in the low field side case, which was thus verified).

- Demonstration that quantitatively different information on transport can be extracted from actively controlled ECR heat pulse experiments compared to that derived from passive methods based on naturally occurring sawteeth.
- Identification of several new MHD phenomena and progress in the quantitative theoretical understanding of them and others (observation of TAE modes also in the absence of fast particles, observation of mode "cascades" of high m/n tearing modes in low or reversed shear discharges, resistive interchange modes in discharges with locally inverted pressure profiles, observation of type-III ELMs in L-mode discharges; quantitative agreement between predictions for neo-classical tearing modes with observed island structure, magnetic field signals and growth rates).

4 PHYSICS AIMS AND MEDIUM TERM PLANS

4.1 Divertor Physics

Edge and divertor physics has been a key element of the ASDEX Upgrade programme from the beginning. In a reactor relevant poloidal divertor magnet system like in ASDEX Upgrade (with the poloidal field coils outside the main field coils) the possible divertor field topologies are constrained. But there is, of course, much freedom with respect to the x-point position and plasma fan orientation, which both depend primarily on the global plasma shape. In addition, however, there is an overwhelming variety of possible target and baffle structures, which can be exploited to optimize the divertor action and its effect on the bulk plasma performance. Depending on the particular situation, one may either aim at a reasonable compromise working over a wide range of plasma shapes and parameters as typical for exploratory experiments, or one may try to find an optimized solution for a particular reference configuration selected for a reactor-grade machine. The ASDEX Upgrade divertor programme up to this points reflects both situations to some extent:

- The initial Divertor I geometry (fig. 2) was a geometrically rather open, simple structure, which was fairly insensitive to x-point movement, but had enough baffling to achieve high recycling as well as acceptable hydrogen and helium pumping over a wide range of parameters.

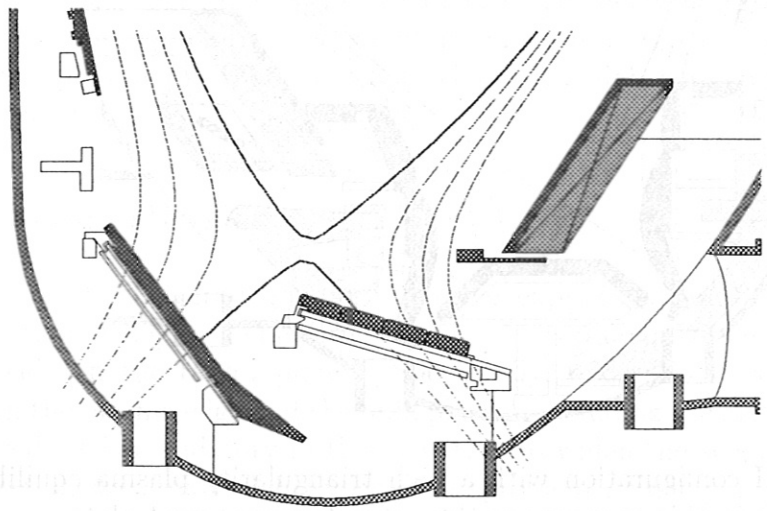

Figure 2: The initial Divertor I geometry.

In contrast, the Divertor II (LYRA, fig. 3) installed in 1996/97 within the voluntary ITER R&D programme, was the result of physical and numerical exploration and optimization studies. Though the data analysis for its initial operation phase is still under way, first results indicate in fact a redistribution of power in the divertor in the sense of a more uniform power load on side walls and a large concomitant reduction of the maximum. To get this optimum, both divertor fans must fairly accurately fit the narrow divertor shape, which at present is designed for a low triangularity ITER-type single null equilibrium.

Despite the high degree of specialization, the LYRA divertor can also be run with much higher triangularity, as envisaged for advanced tokamak scenarios (see below), though at

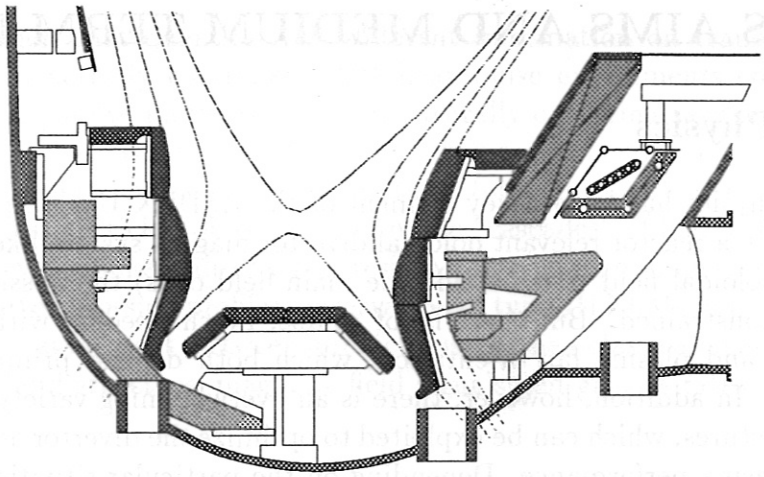

Figure 3: The initial Divertor II geometry (LYRA) with the standard equilibrium (fig. 5 a).

the expense of a reduced divertor action. To accomplish this, a dome baffle with a flat top plate (positioned in the private flux region) has been integrated in the LYRA design, which, in the case of more triangular plasmas, acts as the target plate for the outer divertor leg (fig. 4). During the next summer opening, this dome area will be further "hardened" for high power load by replacing the simple carbon tiles by CFC tiles with hidden edges.

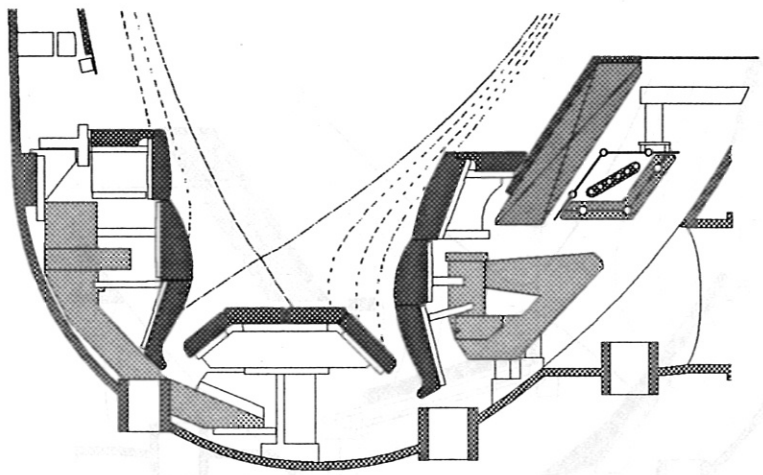

Figure 4: Divertor II configuration with a high triangularity plasma equilibrium (Fig. 5 b). The dome baffle in this case acts as the outer divertor target plate.

The first experiments with Divertor II indicate high performance and high power load capability of this divertor concept. The decision, whether the LYRA divertor should be modified in the near future to implement a further gas-bag variant, as outlined as an option in the Divertor II proposal, will be based on a more thorough analysis of our recent LYRA results and modelling studies.

As mentioned before, tokamak equilibria with moderate triangularity can be run with the presently installed LYRA divertor, though at the expense of a less optimal divertor action with respect to power distribution, neutral recycling and pumping. While this phase will allow the testing of a reasonably wide range of shaped plasma configurations with respect to bulk plasma performance, a more optimized divertor configuration is desired

in the longer run, in order to regain the full divertor benefit for these higher triangularity plasma shapes.

The decision, which way to go, should fully utilize the experinece gained with the LYRA divertor. The LYRA divertor is in operation since early summer 1997, but part of the new and reconstructed diagnostics and the full NBI heating power of 20 MW are available only since late 1997. Therefore, the assessment of the most important physical processes and divertor elements is still premature, but significant progress is expected on a half year time scale, allowing for a decision to be made late in 1998.

At this early stage, however, already three options can be identified:

1) An adaption of the presently installed LYRA, requiring only minor modifications of the dome baffle. Such a modification would be possible in the frame of the running programme.

2) In principle, the excellent performance of the close fitting LYRA divertor in the case of low triangularity should be attainable also at higher triangularity, if the target plates and baffles are readjusted such that their shapes relative to the modified flux surface geometry are retained. However, such a divertor design can optimally fit only a narrow range of triangularities around a mean value to be carefully chosen on the basis of the existing knowledge.

3) Alternatively, a more open, less optimized divertor geometry may be chosen, which might still have acceptable power handling and pumping capability for a much broader range of equilibria, but does not achieve the high performance of a LYRA type arrangement.

4.2 Bulk Plasma Physics

As a result of the ASDEX Upgrade studies and other experiments on SOL- and divertor physics, the operation at high edge densities seems to be a prerequisite for power exhaust with tolerable loads on the target plates. Specifically, under these conditions strong interlinks between the plasma edge and the bulk plasma, including the global confinement, have been observed. It is mandatory in this situation to widen the scope of the ASDEX Upgrade investigations to a more global view of the problems. Edge parameters influence core confinement in various ways. L-mode and H-mode confinement are discriminated by local edge parameters, core confinement is observed to depend on the edge pressure, and confinement enhancement by core density peaking is found in the H-mode regime with high radiated power fraction (CDH-mode). At the same time, edge parameters set boundary conditions for divertor operation, e.g., detachment and density limit windows and power exhaust. Therefore edge physics can only be studied in the context of integrated solutions for the bulk, the edge, and the divertor; this is why ASDEX Upgrade has been addressing progressively the combined study of bulk, edge, and exhaust plasma physics.

In the coming next years, bulk physics studies will concern mainly the energy and particle transport, MHD-instabilities, and their stabilization. Regarding energy transport, in-depth studies concerning the relation between core and edge and their mutual inter-

action, transport barrier physics, dimensionless scalings and heat wave propagations are envisaged.

The investigations of MHD modes like the neoclassical tearing modes, which limit the achievable β in ITER to values well below the Troyon limit, or toroidicity induced Alfvén waves will be continued. Experiments on mode stabilization using ECRH and ECCD have started recently.

Particle transport and density limit remain a substantial part of our effort, including the promising refuelling by pellet injection from the high field side.

Bulk plasma physics studies in the conventional (ITER-base line) operating mode of tokamaks will profit from the planned modifications to the ASDEX Upgrade device and its auxiliary systems.

The two NBI systems will now have different power, particle and momentum deposition profiles (although the total deposited momentum of the two systems will change only little, due to the compensation between the larger tangent radius and the higher particle energy of the second system), and, in particular, different orbit characteristics of the fast particles. This will, for example, affect the MHD behavior.

A more tangential beam injection reduces the number of trapped particles especially in the plasma centre. Taking only the new tangential injector, only those ions which are deposited near the plasma edge (within the outermost 2 or 3 cm) would be born on trapped orbits. That affects especially the fishbones, which, together with the sawtooth crash, might play an important role in providing a seed island for the appearance of neoclassical tearing modes. These slowly growing MHD instabilities are of significant importance in long pulse discharges. Besides the formation of the seed island and its dependence on plasma parameters such as collisionality, the growth of those modes and the resulting saturated island width will be investigated. Furthermore, experiments of an active stabilization of these modes by phased electron cyclotron current drive and heating will be carried out and accompanied by theoretical investigations.

Since the parallel velocities of the fast ions will become larger using the new injector due to both the more tangential injection and the higher injection energies, the coupling between the fast ions and toroidicity induced Alfvén Eigenmodes (TAEs) will become more efficient. Therefore, one expects, the TAEs to be driven more unstable using the new injector, whereas up to now they have been only marginally unstable.

It has been demonstrated in various tokamak experiments, including ASDEX Upgrade, that plasma shaping (especially higher triangularity) can strongly influence the confinement and ELM behaviour in the H-mode, and correspondingly, ITER is being planned with a triangularity of $\delta_{top} = 0.2$ and $\delta_{bottom} = 0.4$.

With the present in-vessel components (ICRH-antennae, PSL) in ASDEX Upgrade only equilibria with small triangularities of $\delta_{top} \leq 0.1$, $\delta_{bottom} \leq 0.3$ (as shown in figure 5 a) can be investigated. Modest triangularities of $\delta_{top} \leq 0.2$, $\delta_{bottom} \leq 0.4$ (fig. 5 b and c) require a modification of the ICRH antennae which is planned for summer 1998. Going to even higher triangularities of $\delta_{top} \geq 0.5$ requires the construction of new ICRH antennae. These antennae will have a larger toroidal dimension, but a smaller poloidal dimension, which will allow to fully exploit the plasma shaping capabilities of ASDEX Upgrade.

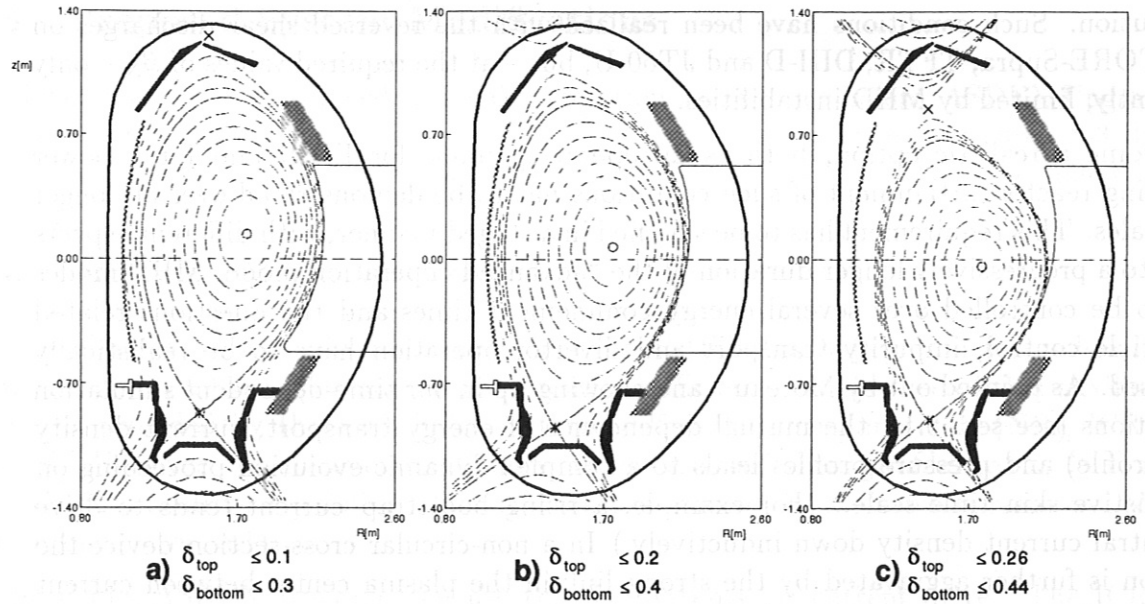

Figure 5: ASDEX Upgrade equilibria with the standard shape (a) and higher triangularity (b and c). The highest triangularity ($\delta_{top} \leq 0.26$, $\delta_{bottom} \leq 0.44$), shown in **c,** can be achieved only with a smaller plasma cross-section.

In a first stage, equilibria with higher triangularity can be run with the present divertor II (see sec. 4.1) and preparatory experiments regarding the effect of plasma shaping and different ramp-up scenarios will be carried out in this manner. For dedicated studies addressing specifically the compatibility of higher triangularity equilibria with the divertor requirements, a further modification of the divertor design might become necessary, as described before in sec. 4.1.

The ideal pressure driven kink mode has been shown to limit the maximum achievable β seriously. Besides profile optimisation (broad pressure profiles) and plasma shaping (high triangularities) this instability can be stabilized by a nearby conducting wall which acts as a perfect conductor for a rotating plasma. In ASDEX Upgrade the walls are fairly far away from the plasma, and their stabilizing influence is rather small. However, the passive stabilizing saddle loops (PSL) in ASDEX Upgrade, required for reducing the growth rate of the vertical instability, could be extended in poloidal direction. Since for high pressure the mode is located mainly at the low field side, a partial wall put here would have a strong stabilizing effect.

4.3 Advanced Tokamak Scenarios

It is now generally recognized that steady state operation with a high bootstrap current fraction is the most promising option for an economically attractive tokamak reactor. This has led to increasing attention being paid to such operating modes in the ITER programme, and in the recognition of the associated physics problems as a central theme of tokamak research for the coming years. To realize "advanced" modes of operation, a tokamak has to achieve high values of β_N, with good energy confinement, and with current and pressure profiles compatible with the intrinsic characteristics of the bootstrap current

distribution. Such conditions have been realized with the reversed shear discharges on JET, TORE-Supra, TFTR, DIII-D and JT60-U, but – at the required values of β_N – only transiently, limited by MHD instabilities.

To become a realistic option, both as an operating mode for ITER and for a power producing reactor, attainment of such conditions has to be demonstrated over all longer time scales. This requirement has to be satisfied in a staged manner, with different aspects linked to a progressively longer duration of the "advanced" operation mode. MHD modes have to be controlled over several energy confinement times and the questions related to particle control, impurity transport and divertor operation have to be realistically addressed. As pointed out by Moreau [3] and showing up in our time-dependent simulation calculations (see sec. 5.1), the mutual dependence of energy transport, current density (or q-profile) and pressure profiles leads to a complex dynamic evolution proceeding on the resistive skin time scale. (For example, a rising bootstrap current tends to drive the central current density down inductively.) In a non-circular cross-section device the situation is further aggravated by the strong link in the plasma center between current density and flux surface shape. Ultimately, also slow secular dynamics proceeding over many skin times and true steady state operating conditions at zero loop voltage will also have to be studied.

ASDEX Upgrade has a large capability for plasma shaping, extensive experience and knowledge of poloidal divertor operation, flexible and powerful heating (NBI, ICRH, ECRH), refuelling (high and low field side pellet injectors) and pumping (both turbo-molecular and cryogenic) systems, and elaborate control and diagnostic systems. This makes ASDEX Upgrade particularly suited to investigate the physics of "advanced tokamak" scenarios. To meet further these goals, it needs a current drive capability and a modest upgrading of its power-supply system to extend the pulse lengths. This will allow the study of questions of divertor physics and particle/impurity control, MHD stability, and discharge dynamics on the time scale of a few skin-times, which are now the most urgent topics for establishing the credibility of "advanced" scenarios.

Correspondingly the goal of the ASDEX Upgrade advanced tokamak program is to

- test operating scenarios
  - freezing of the current profile during current ramp-up,
  - current profile control by current drive (up to 250 kA) (long pulse)
  - fuelling by pellets
- investigate the related bulk physics (MHD stability, mode stabilization, energy and particle transport) and the edge physics including edge-bulk coupling
- achieve stationary profiles, compatible with the advanced tokamak concept (long pulse)
- develop divertor concepts for varying magnetic configurations
- develop the relevant diagnostics.

[3] D. Moreau, 5th European Fusion Physics Workshop, Sesimbra, Portugal, Dec. 1997

4.4 Proposed System Modifications

For investigations of "advanced tokamak" operation, as outlined before, ASDEX Upgrade requires a current drive capability of about 250 kA, and a flattop time of at least 2-3 skin times, i.e., 10 seconds. The modifications necessary for this are described in the following.

4.4.1 Heating and Current Drive

For the above mentioned physics program and the ASDEX Upgrade parameters, a heating power of about 20 MW (already in operation) is sufficient. Flexible use of this auxiliary power is provided by the availability of three different heating methods (NBI, ICRH, ECRH). However, for achieving stationary flat or reversed shear profiles (at $q_0 \geq 1$) an off-axis current drive capability of about 250 kA is required at a plasma current of 1 MA (according to sec. 5.1).

In principle, ASDEX Upgrade can use the RF systems for current drive. The ICRH system (6 MW) is expected to become fully usable for plasma heating after the installation of four 3 db couplers in 1997, while current drive using mode conversion (up to 150 kA off-axis) should be available in 1998. First estimates show that ECCD for ASDEX Upgrade conditions might allow a flexible current drive scheme, but with an efficiency of only 14 kA/MW (off-axis). Therefore the presently available RF systems would not be sufficient to deliver the required current drive of 250 kA. RF current drive of 250 kA would require an extension of the ECRH system to 8 MW. This would demand the use of not yet available 1 MW steady state gyrotrons, large additional installations and high costs.

With regards to NBCD of about 250 kA, two options are possible:

a) Turning the injector 2 (100 keV D^0) into a more tangential] injection direction with all 4 sources still available (2 sources for CD and 2 for heating) results in an only slightly off-axis peaked current drive profile. As the deposition maximum is required to be at $\rho_{pol} \sim 0.5$, the NBI box has to be moved further away from the tokamak. With this geometry, two heating sources inject still radially, and the power exclusively for plasma heating is 15 MW. 5 MW are injected tangentially and procide therefore both, current drive and plasma heating.
At least one year is needed for turning the injector.

b) Installation of a new tangential injector equipped with two sources (100 keV, D^0) would allow optimized off-axis deposition and is less sensitive to the vertical plasma position. This solution, however, would be much more expensive and would need extensive re-arrangement of existing diagnostics.
A long term perspective for such a third injector could be to replace the ion sources – and some additional equipment – by negative ion sources and thereby provide a testbed for the technology of negative ion beams.

NBCD has a rather high current drive efficiency, and some advantages compared with RF, namely
- driving toroidal rotation for mode stabilization,
- no restrictions for operation with respect to coupling requirements.

Therefore NBCD (with option a) will be used as the main tool for current drive on ASDEX Upgrade, and the reasons for choosing option a) are discussed in sec. 6.1 in detail.

The off-axis RF current drive of up to 180 kA presently available will be used for flexibility and additional requirements based on scenario considerations (sec. 5.1).

4.4.2 Reactive Power Compensation

For the programme discussed above, the capabilty for higher triangularity and current drive are necessary technical prerequisites. The more effective generation of highly triangular double-null-like plasma configurations using the available shaping coils requires no higher poloidal field energies. This and the limitation of the additional heating power (including current drive) to 20 MW reveal that at $Ip = 1$ MA the flywheel energy of the two generators EZ3 and EZ4 is sufficient for future ASDEX Upgrade experiments up to a flat top time of ≈ 10 s.

However, the flywheel energy of the generator EZ3 (500 MJ) can only be fully exploited by compensating the reactive power[4] of the Thyristor converters with capacitors. A proper mix of additional heating units, needed only during the flattop phase, and power supplies for the PF field coils will then permit the balancing of the apparent power during the ramp up and flattop phase. Estimates show that a compensation of reactive power up to 120 MVAr will be required for future long pulse experiments.

This should be done in two steps, namely 30 MVAr which is under construction (and not a subject of this proposal) and 90 MVAr which is the matter of this application.

4.5 Time Schedule

Figure 6 shows in the top table an overview of the ASDEX Upgrade short term physics programme. The bottom table indicates the time schedule for those major changes for the medium term programme which are eligible for preferential support and are discussed in this application.

4.6 Collaboration within the European Fusion Programme

The investigations on advanced tokamak operation will be conducted in already existing close collaboration with other EURATOM associations, especially with Culham laboratories on MHD stability, with CEA Cadarache on the control of steady state scenarios, and with JET on current drive and optimisation of steady state scenarios.

[4] **reactive power** is (apparent power^2 - active power^2)$^{1/2}$, where **apparent power** is the ac power ($\sqrt{3}\ U_{eff}\ I_{eff}$), and **active power** is the dc power. The apparent power for the thyristor converters is approximately thyristor zero current voltage U_{dio} times dc current I_d. This power has to be supplied by the ac generator in form of apparent power independent of the required voltage U_d of the dc circuit.

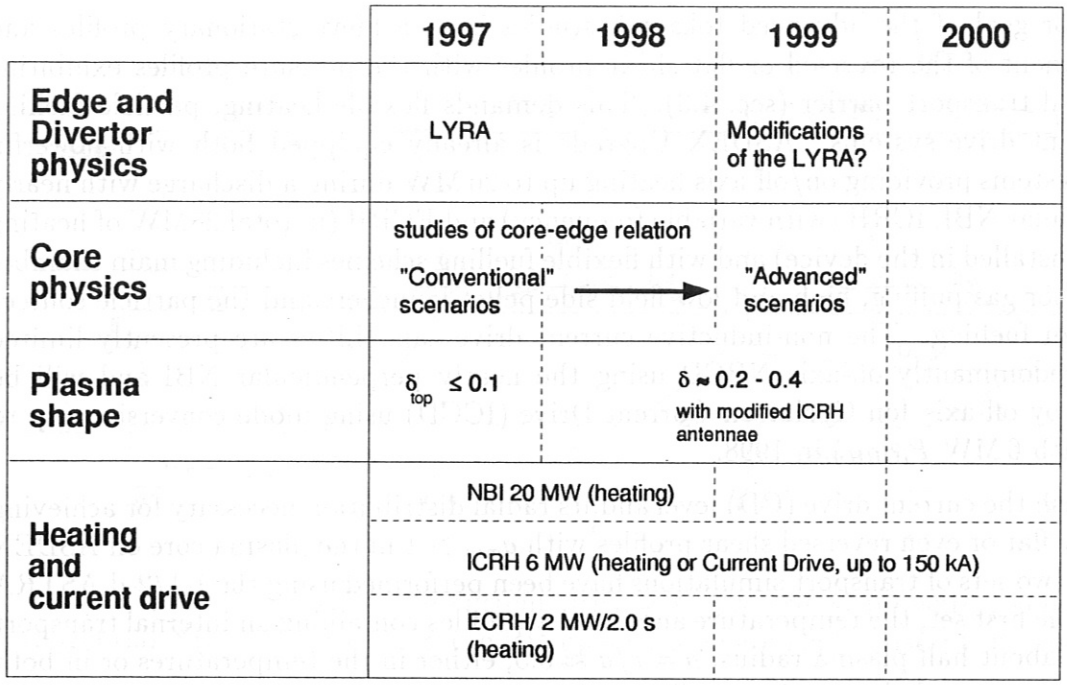

preferential support items

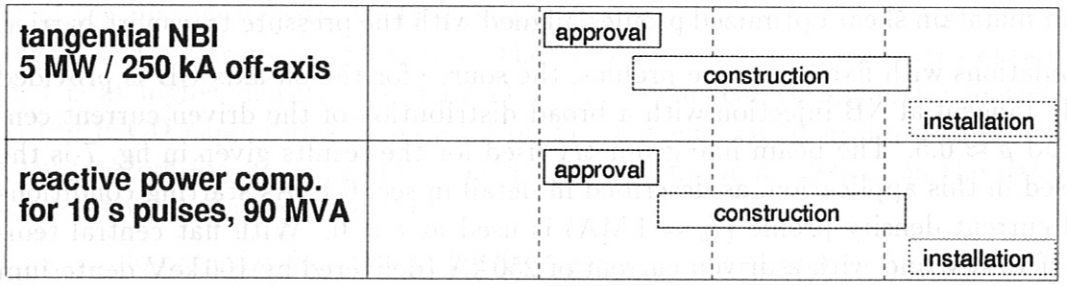

Figure 6: Time table of the short term physics programme on ASDEX Upgrade (top part) and time schedule for preferential support items for the medium term programme (bottom table).

5 REQUIREMENTS FOR MEETING THE OBJECTIVES

5.1 Off-axis Current Drive Requirements for Advanced Tokamak Scenarios

One major goal of the advanced tokamak studies is to achieve stationary profiles and the alignment of the reversed or flat shear profiles with the pressure profiles exhibiting an internal transport barrier (sec. 4.3). This demands flexible heating, particle fuelling and current drive systems. ASDEX Upgrade is already equipped both with powerful heating systems providing on/off axis heating up to 20 MW during a discharge with nearly perpendicular NBI, ICRH (with variable frequency) and ECRH (in total 28MW of heating power is installed in the device) and with flexible fuelling schemes including main chamber and divertor gas puffing, high and low field side pellet launchers and the particle sources from beam fuelling. The non-inductive current drive capabilities are presently limited to the predominantly on-axis NBCD using the nearly perpendicular NBI and will be extended by off-axis Ion Cyclotron Current Drive (ICCD) using mode conversion (up to 150 kA with 6 MW P_{ICRH}) in 1998.

To establish the current drive (CD) level and its radial distribution necessary for achieving stationary flat or even reversed shear profiles with $q_{min} > 1$ in the plasma core on ASDEX Upgrade, two sets of transport simulations have been performed using the 1-1/2-d ASTRA code. In the first set, the temperature and density profiles containing an internal transport barrier at about half plasma radius, $\rho = r/a \approx 0.5$, either in the temperatures or in both the temperature and the density, as observed in present advanced tokamak experiments have been prescribed, and just the current diffusion is simulated (fig. 7 for $I_p = 1$ MA). In the second set, the full transport equations are self-consistently solved, and the heating and CD time scenarios are optimized in the ramp-up and in the current flattop phase to achieve and maintain shear optimized profiles aligned with the pressure transport barrier.

In the simulations with fixed pressure profiles, the source for the off-axis CD is provided by a nearly tangential NB injection with a broad distribution of the driven current centered around $\rho \approx 0.5$. The beam line geometry used for the results given in fig. 7 is the one proposed in this application, as described in detail in sec. 6.1. As starting conditions a reversed current density profile ($I_p = 1$ MA) is used at $t = 0$. With flat central temperatures of 10 keV and with a driven current of 250 kA (delivered by 100 keV deuterium beams with a power of 5 MW) the current profile hardly changes any more after 5 s, becoming truly stationary after 15 s (constant E field across the radius). The bootstrap current is about 700 kA with a strong peak at the position of the high pressure gradient, while the necessary seed current on axis is provided by a small inductively driven ohmic current peaked at the highest plasma temperature. These numbers highlight two mandatory requirements for steady state advanced tokamak operation, namely a high bootstrap current fraction to limit the CD power and – for the creation of the bootstrap current – sufficient pressure gradients created by high confinement properties to limit the heating power required.

The results described are rather insensitive to other assumptions for the plasma para-

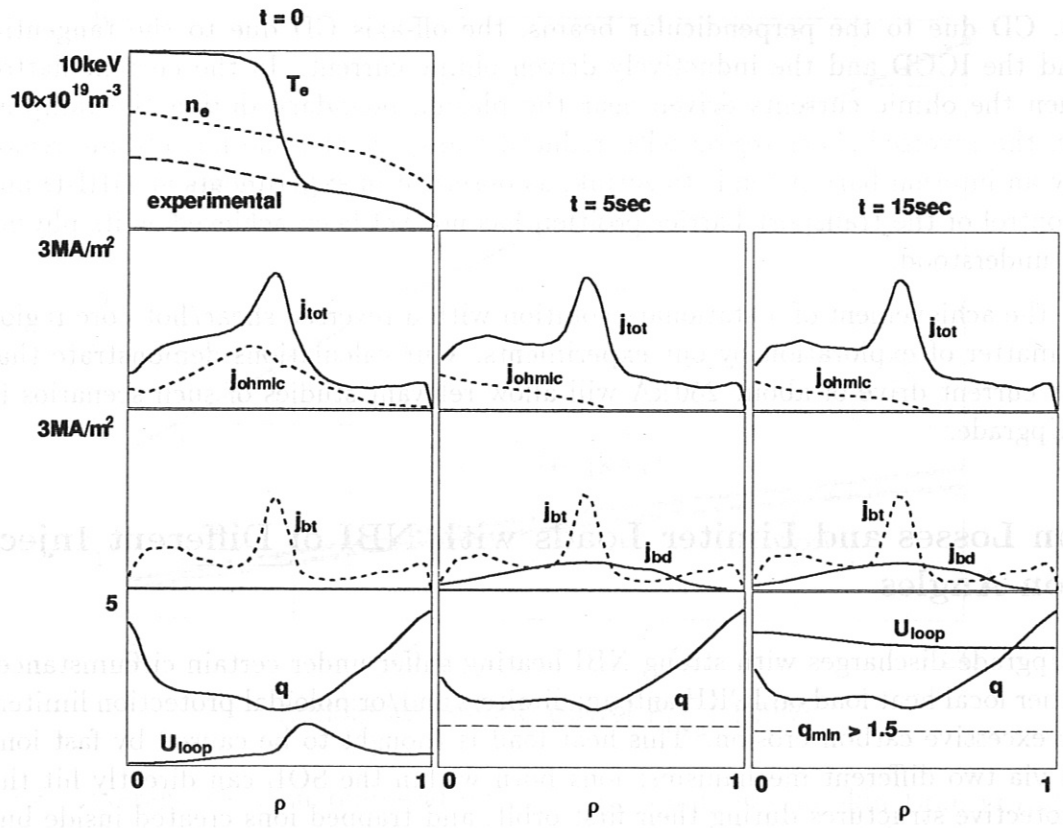

Figure 7: Modelling of neutral beam current drive with prescribed pressure profiles for 5 MW tangential NBI. The profiles in the left upper frame are kept constant in time.

meters. For instance, using density profiles including also a transport barrier, but with the same line averaged density, will not shift the position of the driven current to smaller radii. Changes of the temperature in the region of high CD efficiency around $\rho \approx 0.5$ and/or of the plasma density would need either a higher beam energy (to maintain the coupling to the electrons for $T_e(a/2) \geq 4\,\mathrm{keV}$) or higher beam powers (to obtain high enough CD at higher densities for $T_e(a/2) < 2\,\mathrm{keV}$). Instead of higher tangential beam powers the ICCD capabilities or reduced plasma currents could be used to provide the necessary freedom for experimental investigations. Some more details on the parameter dependencies are discussed in sec. 6.1.

For the scenario optimization, the ASDEX Upgrade conditions for ramp rates of plasma and PF currents as well as of additional heating power schemes are used. The latter include an early preheating with 1 MW ECRH during the current ramp-up to create reversed shear profiles, a stepped increase of the available nearly perpendicular NBI power up to 15 MW to heat the plasma center and the proposed nearly tangential injection up to 5 MW supplemented by up to 150 kA ICCD for on/off-axis current drive to control the current profile. These time dependent scenario calculations are done to prepare operating scenarios and to confirm the results obtained with prescribed pressure profiles. To create the internal transport barrier, both the anomalous thermal conductivities for ions and electrons are switched off inside the reversed/flat shear region with $dq/d\psi \leq 0$ and only the neoclassical contributions are taken. The problem encountered is then given by the time evolution of the bootstrap current driven by the pressure increase due to the reduced

transport, CD due to the perpendicular beams, the off-axis CD due to the tangential beams and the ICCD and the inductively driven ohmic current. In the current flattop phase when the ohmic currents driven near the plasma boundary during the ramp-up disappear, the reversed shear region with reduced transport and the hot plasma region limited by an internal barrier tends to shrink, as observed in experiments at DIII-D and JET. A control of the transport barrier position has not yet been achieved as its physics is not yet understood.

Therefore the achievement of a stationary solution with a reversed shear/hot core region will be a matter of exploration by our experiments. Our calculations demonstrate that an off-axis current drive of about 250 kA will allow relevant studies of such scenarios in ASDEX Upgrade.

5.2 Ion Losses and Limiter Loads with NBI of Different Injection Angles

ASDEX Upgrade discharges with strong NBI heating suffer under certain circumstances from a rather local heat load on ICRH antenna limiters and/or poloidal protection limiters leading to excessive carbon erosion. This heat load is thought to be caused by fast ions from NBI via two different mechanisms: ions born within the SOL can directly hit the nearby protective structures during their first orbit, and trapped ions created inside but close to the separatrix can be rapidly lost by stochastic ripple diffusion. Both first ion orbits and the region of trapped ions depend on the injection angle, but, in different ways. A modification of this angle may therefore help to further clarify the relative contribution of the different fast ion losses and to find an adequate way to reduce their consequences. Present experimental results already indicate that a more tangential injection alleviates the heat load problem.

5.3 Pulse Length and Toroidal Field Requirements

The pulse length required for relevant advanced tokamak studies is governed by the resistive current diffusion time being much longer than the transport time scales both for particles and energy. While these resistive diffusion times can go up to 5 s at high core temperatures of about 10 keV (fig. 7), the use of the current and heating ramp-up phase for establishing near steady state conditions already at the end of the ramp-up phase (see sec. 5.1) mitigates the demands on the relevant length of the flattop phase. Therefore a flattop length of about 2-3 resistive diffusion times, i.e., ≈ 10 s, is considered long enough to study steady state issues of such scenarios and their control.

For this long pulse operation the nominal value of $I_{pN} = 1.4$ MA (possible for up to 4 s flattop length) can be reduced to the long pulse value $I_p = 1$ MA. Though the investigation of advanced scenarios with current drive for sustaining the reversed shear configuration is a main motivation for long pulse operation, the available flux swing of the OH transformer of 9 Vs[5] allows 10 s pulses even without current drive. Figure 8 shows as a function of the heating power for ITER 92P H-mode energy confinement scaling the achievable average

[5](without PF contribution)

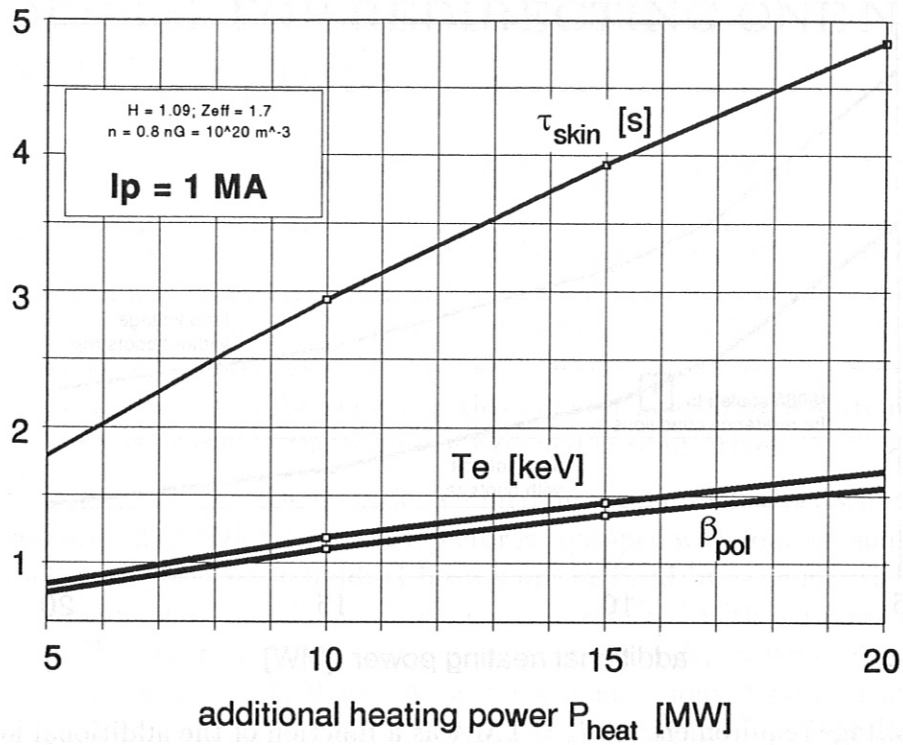

Figure 8: Average electron temperature (T_e), β_{pol}, and plasma skin time (τ_{skin}) as a function of the heating power for operation at 80% of the Greenwald density.

electron temperature, the poloidal β_p and the plasma skin time τ_{skin} at a high density of $\bar{n}_e \approx 10^{20}\,\mathrm{m}^{-3}$, corresponding to 80% of the Greenwald density n_G. The exponents for the parabolic profiles assumed for deriving the plasma resistance and the inner inductance l_i for obtaining the skin time were based on standard experimental H-mode conditions. Thereby the fitting of the plasma thermal energy content resulted in an enhancement factor of $H = 1.09$ relative to the ITER 92P H-mode energy confinement. At the highest powers of $P_{heat} = 20\,\mathrm{MW}$, a $\beta_p \approx 1.5$ would result, being at $B_t = 2\,\mathrm{T}$ above the $\beta_N \approx 2.5$ limit for peaked current density profiles. The available toroidal field level of up to 3 T allows, however, to keep β_N below 2.5, a value which is routinely achieved in ASDEX Upgrade.

The required loop voltage (shown in fig. 9), has been calculated without the bootstrap effect and with the assumption of a bootstrap factor of $f_b = I_{bt}/I_p \sim 0.7\beta_p/\sqrt{\epsilon}$, where ϵ is the plasma aspect ratio. Experimental results indicate that the description with bootstrap current approaches the actual ASDEX Upgrade condition quite accurately. Therefore the lower curve of fig. 9, including the bootstrap effect will be used to judge the flattop time range accessible with the available OH-capability and power supply.

As described in sec. 5.1, necessary ingredients for an advanced tokamak are high confinement (often expressed as confinement enhancement H compared with ITER H-mode confinement scalings) and high bootstrap current fractions. As the bootstrap current fraction scaling can be rewritten as $f_b \sim A^{0.5}\beta_N q_\psi$, a high normalized beta provided by the high confinement at fixed heating power and high q_ψ values are advantageous. To investigate such scenarios up to $q_\psi \approx 5 - 6$, toroidal field operation at up to 3 T should be provided at plasma currents of $I_p \approx 0.8 - 1\,\mathrm{MA}$.

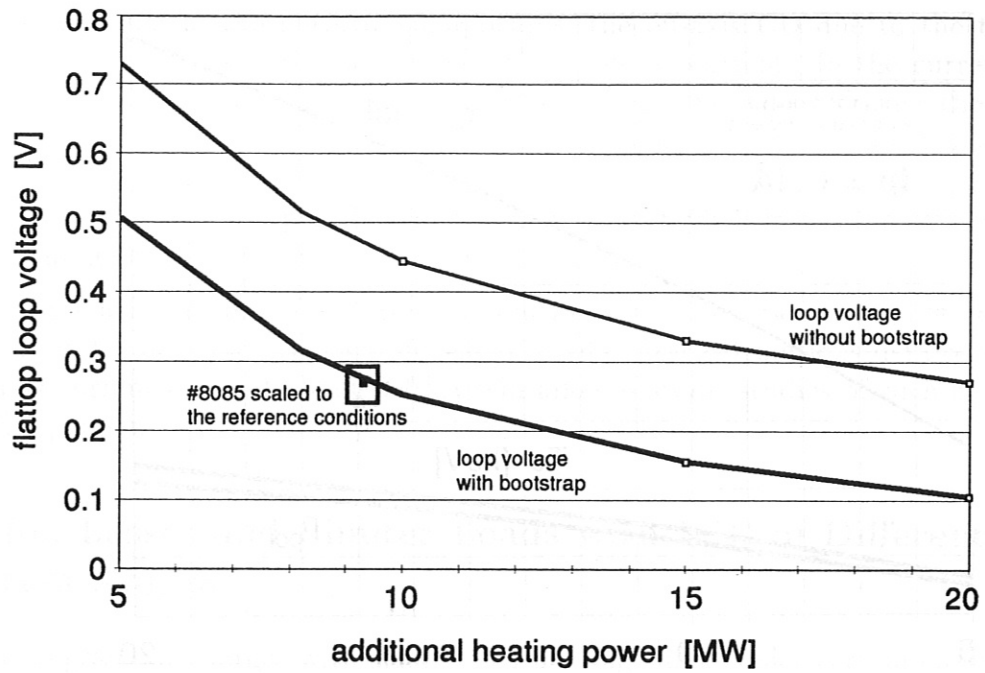

Figure 9: Loop voltage requirement for $I_p = 1$ MA as a function of the additional heating power.

The envisaged 10 second flattop pulses are achievable by means of reactive power compensation with the available power supply, and the technical implications and necessary installations at ASDEX Upgrade will be discussed in sec. 7.

6 PROPOSAL FOR REDIRECTING ONE NEUTRAL BEAM INJECTOR

6.1 Optimization of Beam Line Geometry for Off-axis CD

As discussed in the previous chapter, advanced tokamak experiments on ASDEX Upgrade call in a first step for a non-inductively driven current of about 0.25 MA with a current density peaked off-axis, at about half plasma radius (ρ = r/a = 0.5) and a relatively broad radial distribution. The numbers quoted refer to plasma parameters of $\bar{n}_e = 4 \cdot 10^{19} \mathrm{m}^3$ and T_e (0.5 a) $\approx$ 2 keV. It will be shown in this chapter how these requirements can be fulfilled using neutral beams as the source of external current drive.

Neutral beam current drive (NBCD) is determined by the parallel velocity of non-trapped fast ions. Presently, an ASDEX Upgrade injector is equipped with four ion sources (PINIs) arranged in a rectangle. The individual beams are inclined by $\pm$ 4.90° with respect to horizontal; one pair (the "radial" pair) of beams is injected with a radius of tangency (R_T) of 0.53 m, the other one (the "tangential" pair) with R_T = 0.93 m into a plasma with R_0 = 1.65 m and a = 0.50 m. As a consequence, ions deposited at $R > 1.75$ m (for R_T = 0.53 m) and $R > 1.90$ m (for R_T = 0.93 m), respectively, are borne on trapped orbits. Efficient current drive therefore calls for a more tangential beam injection which will only be possible after modifying the respective ASDEX Upgrade port. Ideally, R_T = 1.32 m is needed in order to avoid trapped particles. However, space restrictions around the tokamak and the requirement of having a sufficiently wide port for beam transmission led to the choice of R_T = 1.29 m. Details of the new port geometry are discussed in the following chapter.

Off-axis current drive obviously calls for off-axis beam deposition. Injection with $R_T \approx R_0 + a/2$ = 1.90 m is impossible as discussed above and a significant non-central deposition with tangential injection is only obtained for high densities at low beam energy (e.g.: $10^{20}\,\mathrm{m}^{-3}$, 50 keV), which is in contradiction to the requirement of current drive. Therefore, the only possibilities to achieve off-axis beam deposition are to increase the beam inclination and/or to move the beam sources further away from the plasma. The simplest modification of the present beam system towards the required geometry would be to leave the internal injector geometry unchanged (β = 4.90°, $R(P_o)$ = 2.84 m) and only move the injector as a whole relative to the plasma, so that the more tangential beams have R_T = 1.29 m. Varying Δx (fig. 10) from - 0.5 m (present value) to positive values allows the degree of off-axis deposition to be changed. However, all results with unchanged injector geometry turned out to be non-satisfactory, since large positive $\Delta x > 1.5$ m (i.e. shifting the present injector away from the tokamak by roughly 2 m) are needed for sufficient off-axis deposition. Under such circumstances the remaining two more perpendicular beams of this injector cannot be transmitted through the port anymore.

A modification of the internal injector geometry is therefore unavoidable. Two cases have been considered in some detail:
(i) $\beta = 5.71°$, $\Delta x = 0$,
(ii) $\beta = 6.65°$, $\Delta x = +\ 1.0$ m,
with R_T = 1.29 m and $R(P_o)$ = 2.84 m being unchanged.

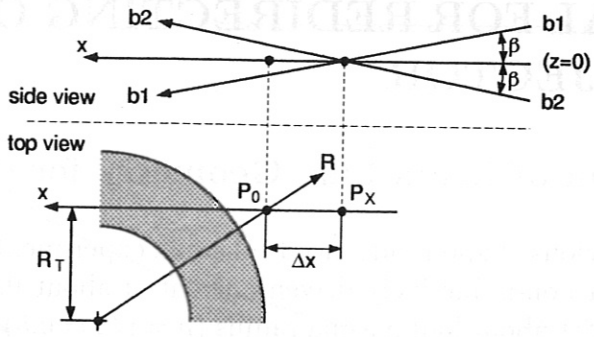

Figure 10: Sketch of neutral beam geometry.

Both cases can be realized within the present injector after some modifications (sec. 6.5) and the remaining two beams can be further used for plasma heating.

The calculation of deposition profiles was performed using the FAFNER code which allows one to model the exact beam geometry as sketched in fig. 10 together with the optics of individual beams. A standard equilibrium of an ASDEX Upgrade discharge was taken; density and temperature profiles could be freely varied. The resulting deposition profiles are normalized such that integration over the plasma volume gives the total injected power minus the shine through. fig. 11 shows the particle deposition profiles for the two cases mentioned above. It is assumed that the two tangential beams are injecting 2.5 MW each at 100 keV (D^0). (For reference, the case presently realized with $\beta = 4.90^o$, $\Delta x = -0.5$ m is included.) The plasma center was assumed to be close to z = 0 and the plasma profiles were taken from measured values.

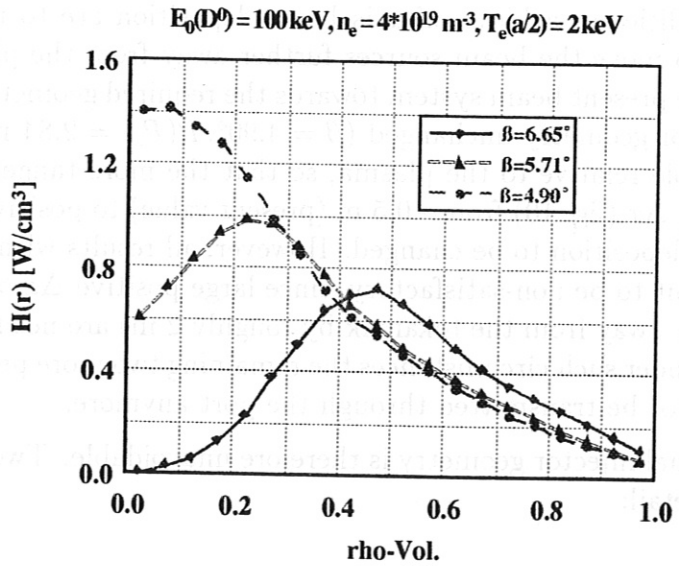

Figure 11: NBI deposition profiles for three different internal injector geometries.

The shape of the deposition profile, especially the position of the off-axis maximum is rather independent of beam and plasma parameters as illustrated in 12, where the results are given for E_{beam} and/or n_e increased by a factor of 2.5.

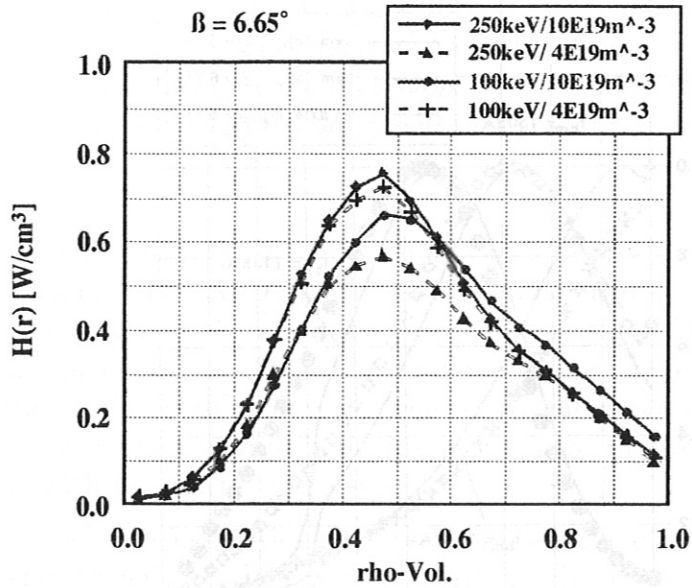

Figure 12: NBI deposition profiles for varying penetration (by factor 6.25).

The relation between beam deposition and beam driven current density for given plasma parameters was studied using the above mentioned ASTRA code. Since the beam geometry in this code is treated in a less detailed manner, the beam input parameters were adjusted such that the resulting deposition profiles are in fair agreement with the above mentioned FAFNER results. Figure 13 compares (normalized) profiles of the beam deposition and of the resulting driven current density for the same plasma parameters as those used to calculate the results in fig. 11. If differences close to the plasma edge are neglected (here trapped orbits and enhanced losses of fast ions may reduce the driven current) beam deposition profiles and beam driven current density profiles closely follow each other, independently of the region where most of the beam ions are deposited. The integrated driven current I_{NBCD}, however, is higher for central current drive, reflecting mainly the T_e-dependence of the current drive efficiency.

In order to determine the parameter dependence of I_{NBCD}, the values of E_{beam}, n_e, T_e and Z_{eff} were varied in different ASTRA runs. The expected $I_{NBCD} \propto 1/n_e$ dependence was verified and further results are given in table 1, where the driven current is normalized to 1 MW of injected power. As already mentioned, a more central beam deposition ($\beta = 5.71^0$) results in a higher I_{NBCD} due to the rather steep T_e profile but the driven current would be too close to the plasma axis. As long as T_e stays relatively low ($T_e(a/2) \approx 2\,\mathrm{keV}$) the current drive efficiency of D^0 beams of 100 keV and 250 keV is similar for the larger inclination angle of $\beta = 6.65^0$. However, when T_e rises to, e.g., twice the standard value ($T_e(a/2) \approx 4\,\mathrm{keV}$), the benefit of higher energy beams becomes evident. Basically this is the consequence of the optimum NBCD energy being dependent on T_e : $E_{opt} \approx (40{-}50)T_e$.

Based on the results summarized in table 1 as well as on the profiles given in fig. 11-13, the choice of the neutral beam parameters proposed for the advanced tokamak experiments

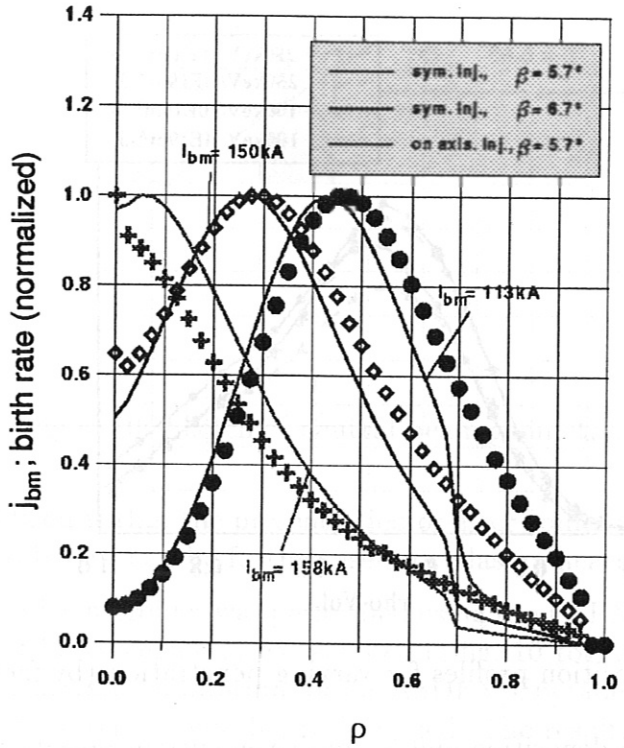

Figure 13: NBI deposition profiles and NBCD profiles.

on ASDEX Upgrade is rather obvious:

- The *beam geometry* characterized by a 6.65° inclination angle (and defined in detail above) results in an off-axis deposition and consequently in an off-axis current drive centered around $\rho = 0.5$ over a wide range of plasma densities.
- A *beam energy* of $\mathrm{E(D^0)} = 100\,\mathrm{keV}$ is adequate as long as T_e at $\rho = 0.5$ remains in the range of 2-3 keV. In other words, a transition to higher beam energies, i.e. negative ion beams will be advantageous only for higher $T_e(a/2) \geq 4\,\mathrm{keV}$. One should keep

E_b	100 keV	250 keV
$Te(a/2)$		
1.8 keV	51	45 (Shine-through limited)
3.6 keV	71 (extrapol.)	98

Table 1: Current drive efficiencies I_{CD}/P_{NI} [kA/MW] for various beam energies E_b and electron temperatures at half radius $T_e(0.5a)$ for a standard plasma of $\bar{n}_e = 4 \times 10^{19}\mathrm{m}^{-3}$, $Z_{eff} = 1.5$.

in mind that 100 kV D^0 beams are envisaged for ASDEX Upgrade in late 1998.

- A *neutral power* of 5 MW at 100 keV D^0 is sufficient to drive the required 0.25 MA. The expected power of the envisaged 100 kV beams is 2.5 MW per beam, however, some 30% of this power is in the $E_o/2$- and $E_o/3$-components. Calculations of the current drive efficiency of these low energy components have shown that the total current driven by the three component beam is still about 85-90% of the one driven by a monoenergetic 100 keV beam. Therefore, re-arranging two of the 100 kV beams to the required current drive geometry will marginally result in the required beam driven current.

So far it has been assumed that the plasma center is kept close to z = 0, i.e., the symmetry plane of the two beams. The ASDEX Upgrade poloidal field system, however, allows equilibria within a widely varying range of the vertical position of the plasma center. In addition, there are other boundary conditions for the choice of the plasma position, set, for example, by the passive stabilizing coils, the ICRH antennae, or the divertor shape. It is therefore of great interest to study how the results given above depend on a vertical shift of the plasma with respect to the beams.

As shown in fig. 14, (left) the deposition profiles of the individual beams (top and bottom, respectively) depend strongly on their relative position with respect to the plasma. The deposition maximum moves from $\rho \approx 0.3$ to 0.6 when shifting the plasma by $\Delta z = 0.12$ m. However, if it is assumed that both beams are injected simultaneously with equal power, the sum of both deposition profiles remains remarkably invariant against vertical plasma shifts over a large range of Δz (fig. 14, right). The proposed beam geometry for off-axis neutral current drive experiments therefore allows a relatively large freedom in choosing the vertical position of the plasma center, a fact which is considered to be of great importance for the investigation of advanced tokamak scenarios.

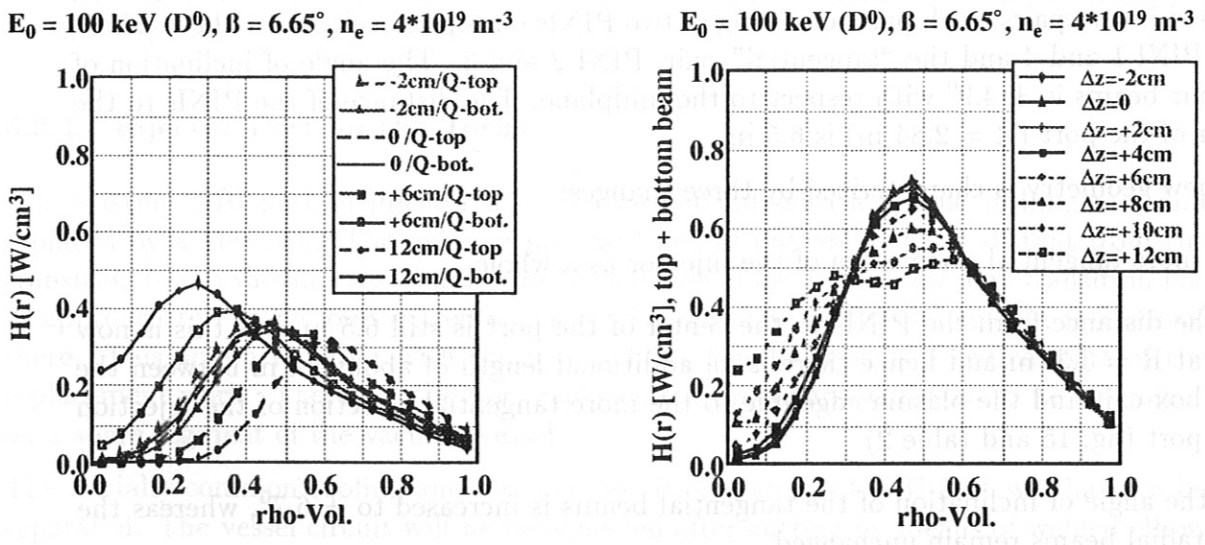

Figure 14: Deposition profiles of individual beams (left) and for the sum of lower and upper beam (right) for varying vertical plasma position.

6.2 Proposed Tangential Neutral Beam Injector (TNBI)

As described before in sec. 6.1, the following physics requirements must be met by the technical concept:

- neutral power: $2 \times 2.5 = 5\,\mathrm{MW}$
- energy: $100\,\mathrm{keV}$ D^0
- radius of tangency: 1.29 m
- angle of inclination: $\pm\ 6.7^0$ with respect to the horizontal mid-plane

The particular choice of the radius of tangency represents a compromise between physics performance on the one hand (CD efficiency, circulating ion fraction) and technical effort on the other hand (acceptable port width for beam transmission). The resulting design offers a net horizontal port width of $\approx 370\,\mathrm{mm}$, however at the expense of several changes on the tokamak structure and an increase of the unpumped duct length by about 500 mm.

As described in sec. 4.4.1, the realization of the above requirements would necessitate either adding a third injector or modifying the second injector, which is the only one suited for 100 keV. The latter alternative has been chosen for the following reasons:

(i) not more than 20 MW of NBI heating power are needed at any one time in ASDEX Upgrade at present;

(ii) a third injector would have been significantly more expensive than a modification of the second one and would have meant a considerably higher involvement of rearranging diagnostics and other equipment in the torus hall.

In order to describe the basic modifications of the second injector, it may be useful to briefly review the present setup (sec. 6.1). There are four PINIs[6] mounted on the injector, grouped in two pairs, each pair consisting of two PINIs on top of each other: the "radial" pair, PINI 1 and 4 and the "tangential" pair, PINI 2 and 3. The angle of inclination of the four beams is $\pm\ 4.9^0$ with respect to the midplane. The distance of the PINIs to the center of the port (R = 2.84 m) is 6.5 m.

The new geometry is characterized by three changes:

(i) a more tangential orientation of the injector as a whole,

(ii) the distance from the PINIs to the center of the port is still 6.5 m, but this is now at R = 3.30 m and hence there is an additional length of about 0.5 m between the box exit and the plasma edge due to the more tangential direction of the injection port (fig. 15 and table 2)

(iii) the angle of inclination of the tangential beams is increased to $\pm\ 6.7^0$, whereas the radial beams remain unchanged.

The first two changes concern the position of the injector as a whole, the third change of course requires internal modifications inside the injector. All these changes are described in more detail in the next three Sections (6.3 – 6.5).

[6] PINI = Plug-In Neutral Injector

$R_T(m)$	radial PINIs #1 and #4	tangential PINIs #2 and #3
old	0.53	0.93
new	0.84	1.29

Table 2: Old and new radii of tangency.

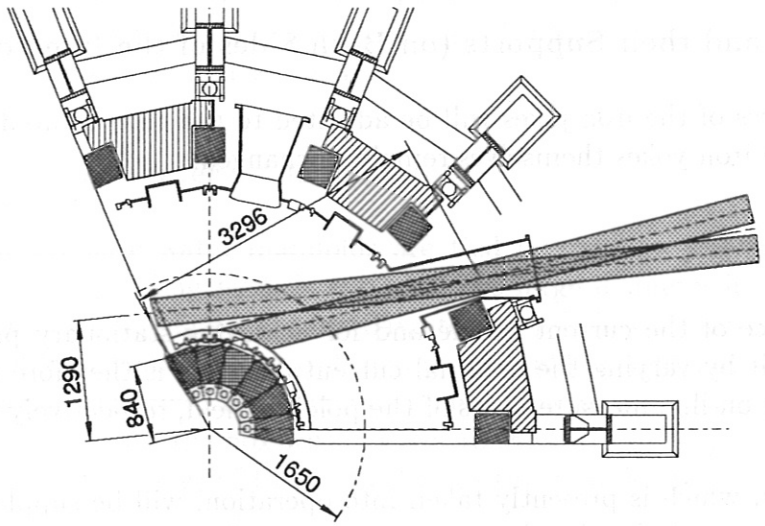

Figure 15: Injection port for NBCD (plane view).

6.3 Modifications on ASDEX Upgrade

Moving the whole injector in the way described requires a number of modifications on ASDEX Upgrade:

6.3.1 Injector Port on the Torus

The existing NBI port of injector 2 has to be cut out with a special milling tool and replaced by a new one. The existing port will be cut out about 6 cm distant from the transition to the vacuum vessel wall. On the left side of fig. 15 the new port transition has to approach the vessel joint extremely close. Therefore an additional cut out is required there. This action together with the new weld at this location is a critical part of the replacement work. Therefore the port replacement procedure will have to be optimized on a spare segment of the vacuum vessel.

The initially common cooling and heating circuit of vessel and NBI port will have to be separated. The vessel circuit will be reconnected after cutting by means of welded elbow joints. The new port will receive an independent cooling and heating circuit.

6.3.2 Vertical Field Coil and Structure Supports

The existing vertical beams, connecting the upper and lower star of the poloidal field coil support structure, will be replaced by new beams with U-bends. The U-bends provide the clearance to the NBI port without reduction of stiffness, since they are manufactured with a larger profile cross section. Exchange and mounting of the new beams require special mounting devices.

6.3.3 Iron Yokes and their Supports (on Both Sides of the Injector)

The support structures of the iron jokes will be adjusted to the new, rotated position of the NB injector. The iron yokes themselves remain unchanged.

6.3.4 Diagnostics for Control

To study the influence of the current profile and for achieving stationary profiles, it is necessary to control it by varying the external current drive. It is therefore essential to have reliable tools for on-line measurements of the poloidal field, respectively the current profile.

The MSE diagnostics, which is presently taken into operation, will be supplemented by another 5 channels, especially for the plasma edge region, to improve the resolution of the measurements. In the same context, the magnetic diagnostics will be upgraded by adding additional sensors.

Using the well established function parametrisation algorithm, the input of both diagnostics will be used for an on-line determination of the current profile, which in turn will be used for feedback control of the driven current.

6.4 External Injector Modifications

The majority of external modifications concern the injector rather than ASDEX Upgrade itself:

6.4.1 Adapter/Interface

Due to the more tangential injection geometry, the present adapter interface between the box/valve exit and the injector port is no longer suitable. A new unit, which is much shorter and has parallel flanges, is required. Internal to the adapter and the new injector port protective and scraping/defining elements are required, partly inertial graphite tiles, partly water-cooled copper and graphite/TZM structures.

6.4.2 Injector Support

The present box support structure cannot be re-used because of the complicated 3D environment in the basement of the torus hall. A completely new support has to be

adapted to the different boundary conditions in the new box position.

6.4.3 Ion Source Shield/High Voltage Cage

Because sources #2 and #3 are now further apart in the vertical direction, the present ion source magnetic shielding must be re-designed in order to take into account the new geometry with respect to voltage stand-off. Consequentially the corresponding support also has to be replaced. The high voltage cage and its support have to be modified to some extent; it is anticipated that it can be extended sideways in order to accommodate the modified high voltage, rf, and water feeds.

6.4.4 High Pressure Water Connections

Whereas the low pressure water manifolds are tied to the box and therefore only an extension of the corresponding feeds is required, the large diameter high pressure feeds are fixed to the torus hall. The 150 mm diameter flexible hoses supplying the movable calorimeter cannot be extended because of their considerable weight and the corresponding torque on the calorimeter drive. It is therefore unavoidable to move the main vertical high pressure feeds together with the box with respect to the torus hall by about 1 m. Due to the large diameter (250 mm Φ) of the vertical feeds this a major task.

6.4.5 Vacuum, Power and other Connections

The vacuum lines from the turbo- to the fore pumps and all the power cables (high voltage, rf, magnet, Ti pumps) must be modified.
Furthermore the control and diagnostic connections have to adapted. Since most of the connections are made by plugs and sockets, this is not worth mentioning except for those cases where cables have to be replaced because they are too short for the new box position.

6.5 Internal Injector Modifications

According to the concept described above, the tangential PINIs (#2 and #3) in the second injector will be oriented such that the angles of inclination with respect to the midplane increases from $\pm$ 4.9^0 to $\pm$ 6.7^0. This is accomplished by two means:
(i) the vertical elevation of those two PINIs above and below the midplane is increased from presently $\pm$ 0.6 m to now $\pm$ 0.7 m;
(ii) the cross-over point of the two beams in the side view is reduced from now 7.0 m to 6.0 m (fig. 10).

A side view of the injector, indicating the new positions of the tangential pair of PINIs, is shown in fig. 16, comparing the old and new geometry.

The internal injector modifications concern the following components:

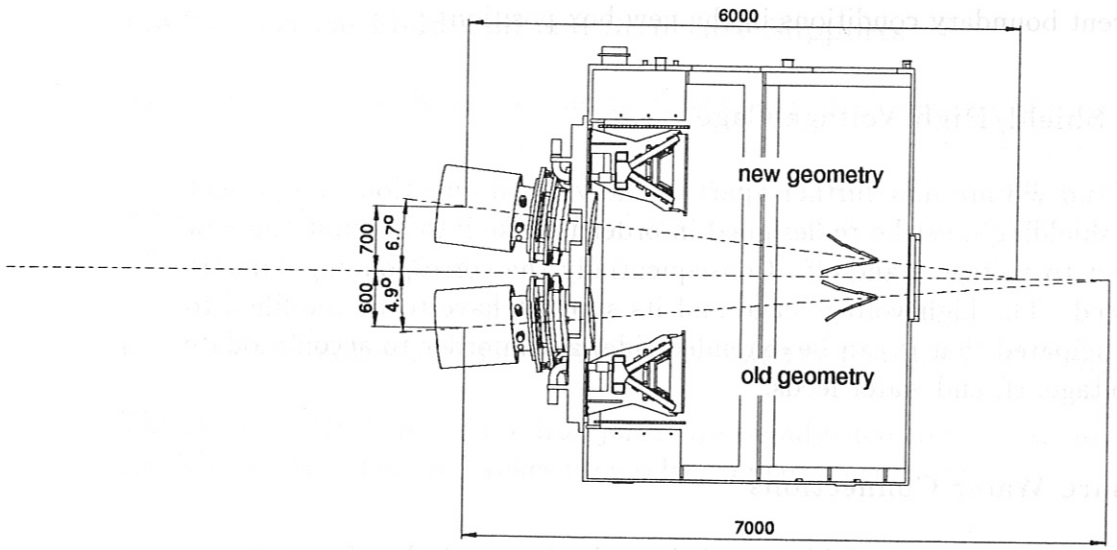

Figure 16: Side view of the NBCD injector internal geometry (still used for PINI #1 and #4) with the old geometry shown in the lower part of the figure, and the new geometry (PINI #2 and #3) in the upper part.

6.5.1 The PINI Flange

Clearly, due to the different positions of the PINIs #2 and #3 and the subsequent neutralizers, the corresponding positions of the ion dumps will also change, and hence a new PINI flange will be required.

6.5.2 The Ion Removal System

Since now two of the beams enter and leave the magnet at higher vertical elevation and under different angles of inclination, the ion orbits will be different. In particular, when leaving the magnet, the reflected ion beams may travel through regions where the magnetic field is non-uniform, and consequently the footprints of the ion orbits, i.e., the power density distribution on the ion dumps may change. Because of the high power densities on the panels ($p_\perp < 25\,\mathrm{MW/m^2}$) of the ion dumps, particular attention has to be paid to the problem of the exact ion orbits in the 3D distribution of the magnetic field. As in the original design the effect of the ASDEX Upgrade stray field, its partial shielding by the main yokes outside the injector, and the gas distribution including space charge electric fields have to be taken into account. To this end the entire ion removal system including all of its 3D-details has been recalculated using the ion orbit tracking code "TRQR" (J. Sielanko et al., to be published) for the evaluation of power density profiles on the panels.

The somewhat unexpected results show that the magnet needs only minor modifications, since apparently the magnet yokes are just high enough in order to ensure that the outermost ion orbits are bent around sufficiently. Some modifications, however, are required for the position of the H_2^+ ion dumps and the magnet liners.

The ion dumps have to be modified in the area of the inertial wings, in order to avoid a

collision with the neutralizers. Since the local angles of inclination change slightly, the position and shape of the inertial liners have to take into account the modified power distribution as well.

As can be seen from fig. 16, the space inside the injector in the vertical direction is limited by the presence of the internal magnetic shielding. However, the space available seems just sufficient for the ion orbits and ion dumps not to interfere with the shielding.

In conclusion, the design power density limit of the water-cooled panels is expected not to be exceeded anywhere on the ion dumps, if the changes described above are performed. However, since the design is not yet complete, some further modifications may still turn out to be necessary.

6.5.3 The Calorimeter

As a consequence of the modified internal geometry, the two beams are now closer together in the vertical direction when they hit the beam line calorimeter. The corresponding change represents a formidable task, since the actively and inertially cooled panels, the water feeds, and the instrumentation are tightly packed together in the present design already. However, the design studies carried out so far indicate that the problem can be solved. This requires the redesign of the complete central calorimeter assembly incorporating the actively and inertially cooled panels as well as the water feeds and the support structures.

6.5.4 The Box-Exit-Scraper (BES)

Due to the somewhat different beam geometry at the exit of the box the BES also has to take into account the different power density profile. It is anticipated, however, that will be possible to modify the existing BES rather than manufacturing a completely new scraper.

Generally, one has to note that this proposal concerns the modification of a used system. Hence, components which have a finite life time, in particular the thermally heavily stressed ones, will have to be replaced for safety reasons if they turn out to be worn out.

7 PROPOSAL FOR REACTIVE POWER COMPENSATION

Long pulse operation in ASDEX Upgrade allows the assessment of advanced scenarios at near steady state conditions with respect to the plasma current density profile (sec. 5.3).

However, for achieving the required flattop time of 10 s at $I_p = 1$ MA with the installed flywheel energy of the poloidal field (PF) generators EZ3 and EZ4 compensation of reactive power is required for the EZ3 generator.

In the following, first the factors limiting the flattop time at $I_p = 1$ MA are summarized, then the amount of reacitve power to be compensated is derived. Finally, the technical effort for installing this reactive power is described.

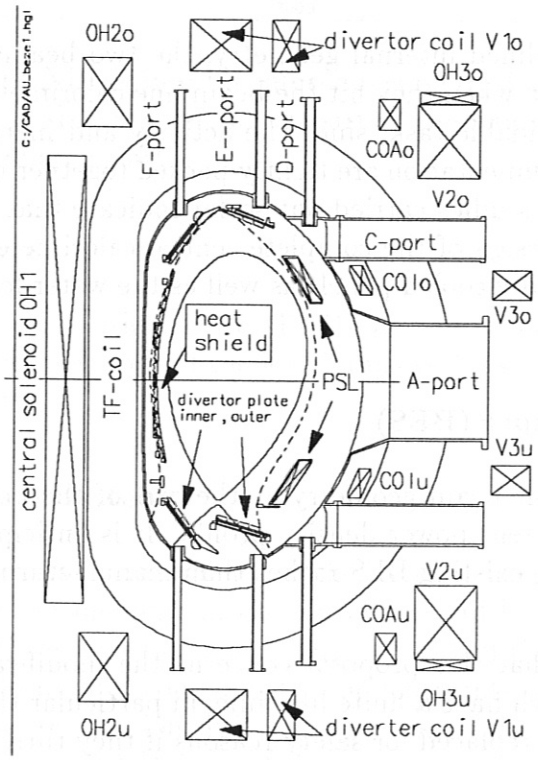

Figure 17: Coil set of ASDEX Upgrade (The drawing still shows divertor I, although divertor II is already in operation).

7.1 Limitations for Long Pulse Operation (Flattop Time)

For $I_p = 1$ MA the adiabatic temperature rise of the ASDEX Upgrade coil set (fig. 17) would permit 20 s pulses (sec. 7.1.1) and thus full steady state conditions with respect to the plasma current density profile. In-vessel components, auxiliary heating and power supplies are compatible with 10 s pulses, as will be described in sec. 7.1.1-7.1.3, and for long pulse operation at $I_p = 1$ MA there are no constraints by magnetic forces. The most stringent limitation for ASDEX Upgrade long pulse operation is the scarce fly wheel energy of the existing generator power supply (fig. 22) for generating the poloidal field

(PF). This will be discussed in sec. 7.1.4. According to this limitation the flattop time of long pulse discharges is limited to the range of 9.5 s to 12 s for 1 MA plasma current, depending on the amount of additional heating power. As a reference value a flattop time of $t_{ft} = 10$ s will be quoted for the long pulse operation envisaged within the scope of this preferential support application.

7.1.1 Coil Set

The COI position control coils (fig. 17) are not considered with respect to thermal limitations, since during flattop the COI currents can be kept at a modest level thanks to the superimposed additional plasma equilibrium control system acting with increased response time on the PF-coils. The remaining coil set comprises the toroidal field (TF) coils, the poloidal field (PF) coils, and the OH-transformer coils. The allowable temperature rise of these coils is the most fundamental limitation of long pulse performance for ASDEX Upgrade, since it directly interferes with the design concept of the core experiment. But nevertheless, pulsed adiabatic operation with LN2 pre-cooling could considerably extend the flattop time.

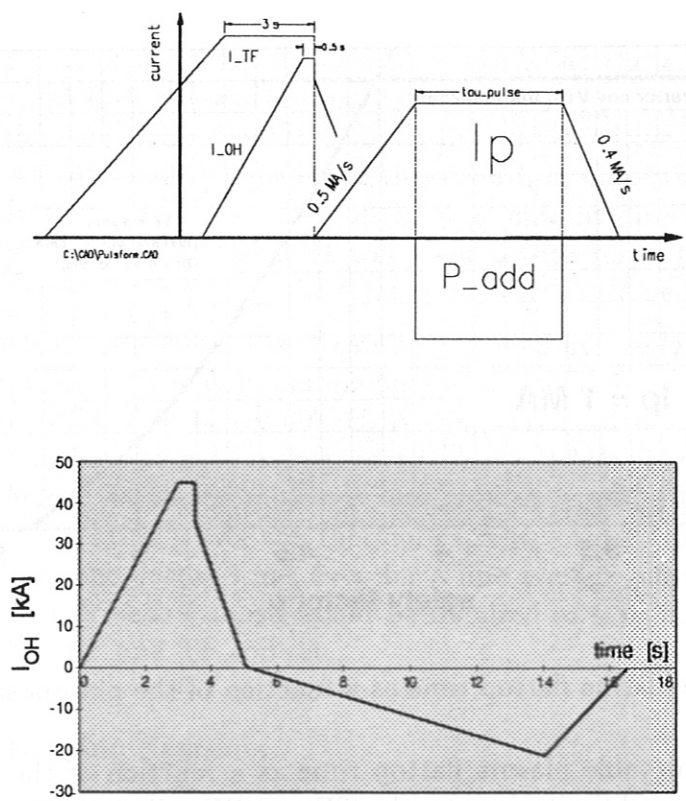

Figure 18: OH-transformer current characteristics.

For evaluating the demands on the power supply for achieving a certain plasma flattop time, the current shapes of fig. 18 have been assumed. These shapes are consistent with the experimental requirements. In particular, the shift in ramp up between TF and plasma current increases the temperature rise of the TF-coils significantly. Also the flattop time of 0.5 s after ramp up of the OH-transformer contributes essentially to its temperature rise.

The flattop current levels for the PF-coils consistent with the plasma current $I_p = 1\,\mathrm{MA}$ are shown in table 3.

Coil	flattop current [kA]
V1o	12.88
V1u	29.06
V2o	-8.13
V2u	-18.13
V3o/V3u	-5.38
COIo/COIu	12
OH2u	15

Table 3: Flattop currents of the poloidal field coils for $I_p = 1\,\mathrm{MA}$.

TF-Coils and PF-Coils

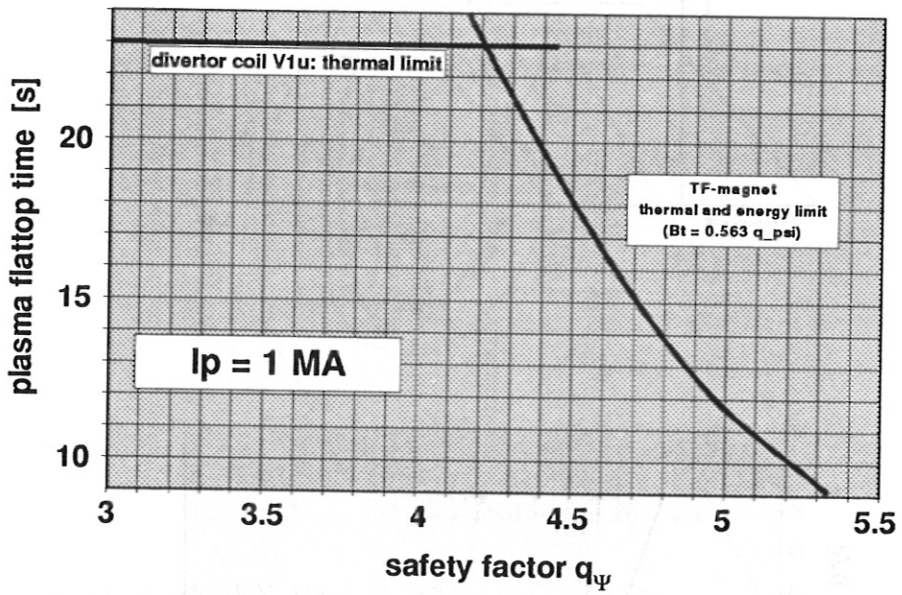

Figure 19: Achievable plasma flattop time as a function of the plasma safety factor.

Figure 19 shows the achievable plasma flattop time as a function of the plasma safety factor q_ψ, if only the thermal limitations by the TF and PF coils are taken into account. Flattop time limitations by the TF magnet are only relevant for $q_\psi > 4.2$, since below this value the adiabatic temperature rise of the divertor coil V1u is more critical. The V1u coil limits the flattop time to roughly 20 s or 4 plasma skin times. Hence 20 s of flattop time is the potential of ASDEX Upgrade accessible with $q_\psi < 4.4$ for $I_p = 1\,\mathrm{MA}$. At the reference flattop time of $t_{ft} = 10\,\mathrm{s}$, the TF-magnet is still capable of providing a q_ψ value as high as $q_\psi = 5.2$ ($B_t \approx 3\,\mathrm{T}$ for a low triangularity plasma shape).

For the TF coils the flattop time limitations given by the temperature rise and the fly

wheel energy (1.45 GJ) of the generator EZ2 are practically identical. Hence the generator EZ2 is the optimum power supply for the TF magnet.

For the PF-circuits the energy supply conditions are much less favorable. An additional stored energy of about 1.4 GJ would be required to fully exploit their thermal capacity. Hence the PF power supply is the bottle neck which limits the ASDEX Upgrade long pulse capability to less than 50% of its capacity (given by the thermal limits).

OH-Transformer

The assumptions for calculating the power and energy demands of the OH-transformer are:

- plasma current break down requires an OH current change of 9.8 kA, which raises the plasma current steeply to 240 kA.
- further ramp up requires an OH current change of 46 kA per MA of plasma current rise.
- during flattop the OH current change per volt second flux change is 10 kA.

The magnetizing current of the OH-transformer is 45 kA. At the end of plasma ramp up to I_p the OH-current just crosses the zero current line in fig. 18, bottom part. This feature would provide a favorable condition for future current drive investigations. For the thyristor converter of the OH transformer this condition makes sure, that there are no temperature limitations, since each unit of the dual current direction converters has almost the same heat capacity as the OH1 coil. Thus, with respect to the OH-circuit temperature rise by Joule heating, only the OH1-coil is the bottle neck.

Fig. 20 shows the flattop loop voltage that can be provided by the OH transformer as a function of the flattop time. The only parameter taken into account is the temperature rise in the OH1 coil, to be kept below 60^0 C. A comparison with the bottom curve of fig. 9 shows that for an additional heating power above 15 MW there is no limitation of the flattop time below the maximum value of 20 s considered in fig. 20. This means that with the available heating power the thermal capacity of the OH transformer is no additional constraint on the flattop time, even for a line average plasma density as high as $10^{20}\mathrm{m}^{-3}$. No current drive assistance would be required to take full advantage of the thermal capacity of the PF and TF coil set.

7.1.2 Auxiliary Heating Systems

The neutral beam heating sources and the ICRH antennas are designed for 10 s pulse duration at full rating. The pulse duration of ECRH gyrotrons (presently increased to a total power of 2 MW) is 2 s. For long pulse operation thus only NBI and ICRH are to be considered. Since the neutral injectors NI1 and NI2 presently in operation with 60 keV sources require about 50% more power than ICRH all computations were carried out for the higher power demand of NBI. The envisaged upgrade of NI2 to 100 keV sources has not been taken into account.

The power factors assumed for 60 keV D2 injection are

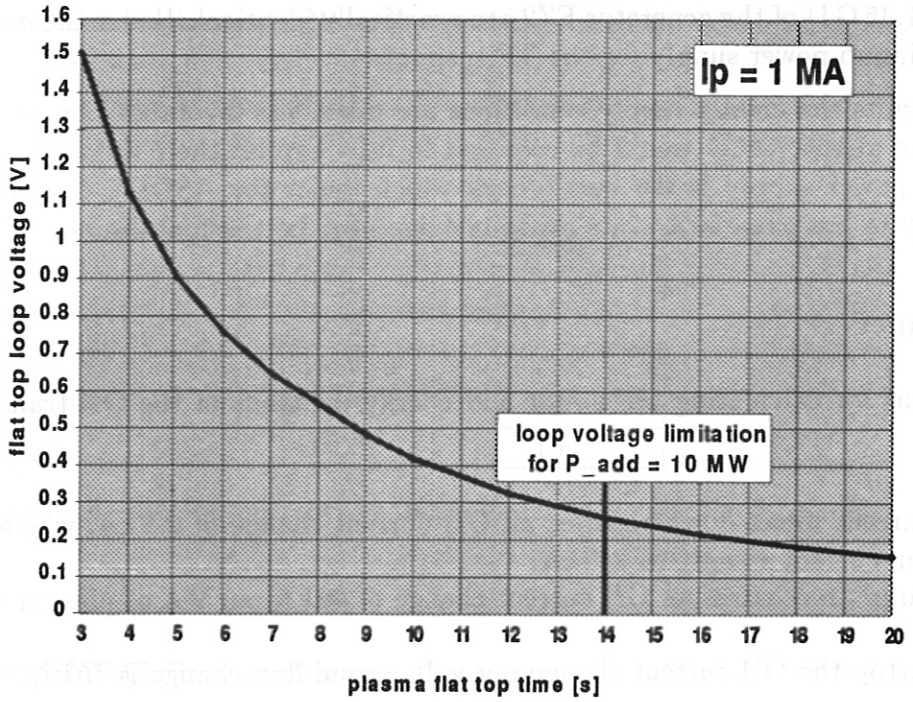

Figure 20: Available loop voltage of the OH transformer as a function of the plasma flattop time.

- active power / nominal power into plasma = 3.5
- apparent power / nominal power into plasma = 5.1

The power demand of the 100 keV sources is about 50% higher.

7.1.3 Power Supply Systems

Generators and power converters are basically designed for steady state operation. For pulsed operation their rating has been significantly increased. As a consequence, their power-on time is determined by the adiabatic temperature rise.

The high voltage converters feed the additional heating systems. Their effective pulse duration is presently limited to 15 s.

The most critical thyristor converter is the one feeding the V1u coil. This converter is adequate for up to 10 s pulses at I_p. A system of further thyristor converter units will have to be ordered in 1998 for back up purposes. If required, one of these 1.2 kV/22.5 kA units could be switched in parallel to a critical converter in order to extend the pulse duration. For the present V1u converter this would be required for pulses longer than 10 s, and for the V1o converter for pulses longer than 15 s.

7.1.4 PF Generators

The existing PF power supply (fig. 22) consists of two generators with rather different properties.

- the EZ4 generator has a flywheel energy of 650 MJ and a short pulse apparent power of 260 MVA.
- the EZ3 generator has a flywheel energy of 500 MJ and a short pulse apparent power of 144 MVA.

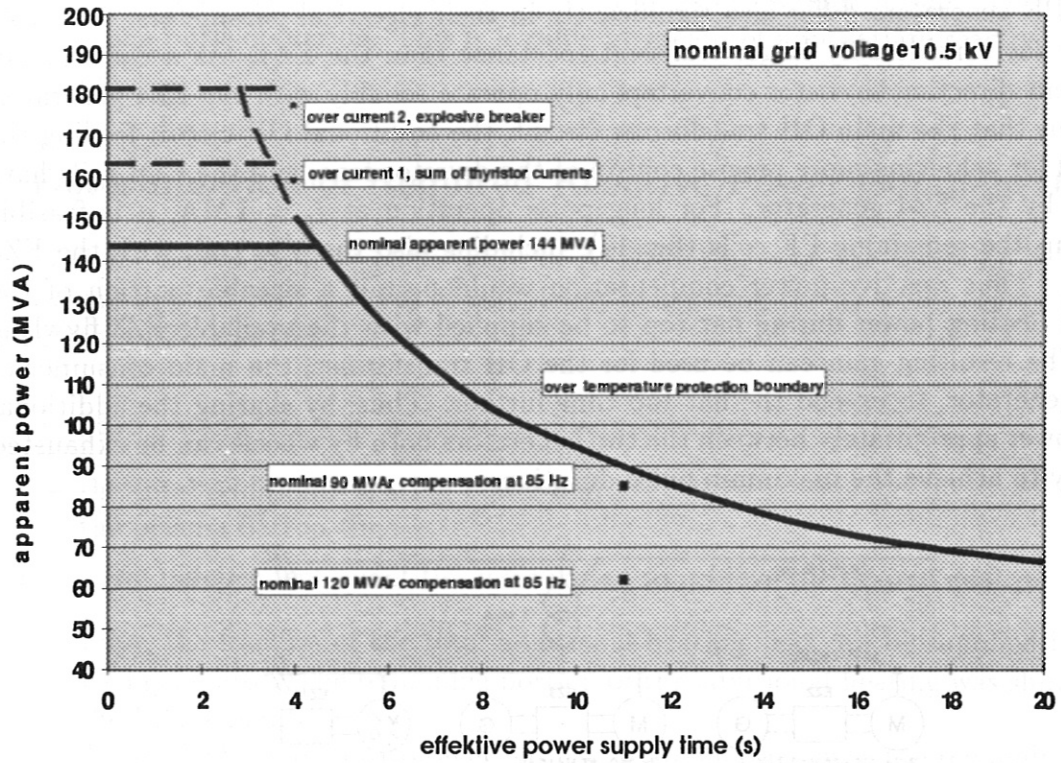

Figure 21: EZ3 generator: Apparent power as a function of the effective power supply time.

The EZ3 flywheel energy is comparable with that of the EZ4 but the apparent power is considerably less. Hence, reduction of part of the apparent power load by compensating reactive thyristor power via capacitors is required for this generator to take full advantage of the available flywheel energy.

Because of the large inductive voltage components required during plasma ignition and ramp-up, the power conversion by thyristors leads generally to a large reactive load component for the generator and in turn to a large apparent power. The reactive power reaches its maximum at flattop, where the high ramp up voltage level of the coil circuits is no longer required but the coil current has reached its maximum value. As a consequence the power factor, defined as $\cos\phi$ = active power/apparent power, becomes very small. In the long pulse case without reactive power compensation, the EZ3 power factor at the end of plasma ramp up is typically $\cos\phi \approx 0.6$. At full flat top the power factor drops to $\cos\phi \approx 0.2$. Reactive power compensation opens thus the possibility to supply additional heating systems, which are required only during flattop.to be

For short pulses of 4-5 s duration the generators provide their full nominal apparent power rating. For those pulses the flywheel energy is not the limiting factor. Therefore part of the EZ3 load, the coil V1o, can be shifted to the EZ4 grid, which is able to provide

the resulting increase in apparent power. The nominal plasma current $I_{pN} = 1.4\,\mathrm{MA}$ can thus be supplied by compensating only 30 MVAr of reactive EZ3 power at 100 Hz via capacitors. For this purpose a pilot capacitor module with 30 MVAr/100 Hz has already been ordered in late 1997. (This module is not part of the preferential support application).

The two PF generators differ also significantly in their electrical parameters. The EZ3 generator has considerably larger transient reactance than the EZ4. As a consequence dual current direction thyristor converters only operate reliably with the EZ4 generator. This means that the main OH transformer circuit, the additional OH circuit feeding the OH2u coil for achieving more precise control of the divertor fans, and the COI coils have to be fed by the EZ4 generator. For long pulse operation at $I_p = 1\,\mathrm{MA}$, it is feasible to ramp up the remaining PF coils (fig. 17), including also the V1o coil, with the EZ3 generator. Thus reactive power compensation would permit a sizeable portion of the additional heating power during flat top to be supplied with the available EZ3 flywheel energy. The resulting gain can be used for the OH transformer, the main consumer of the EZ4 generator, to extend the flat top time further. Thus, by sharing the additional heating power appropriately between the two generators both fly wheels can be exhausted completely to achieve the maximum pulse duration.

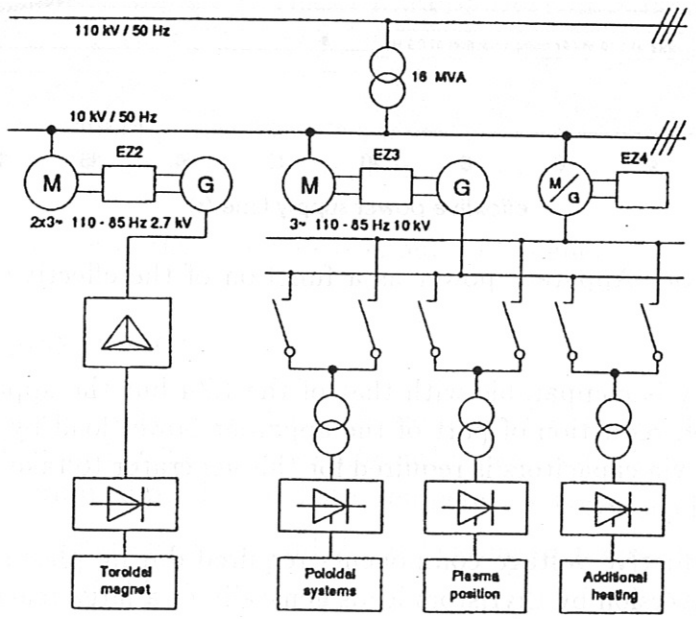

Figure 22: ASDEX Upgrade power supply block diagram.

The two separated grids for EZ3 and EZ4 (fig. 22) do not permit a load sharing as smooth as assumed for the optimisation computations. There are always portions of several MVA which have to be transferred, so that the results gained are somewhat optimistic. However, computations with the special purpose code SIMPLORER will be started to assess the conditions for merging the two 10.5 kV grids. It will be required to study the control features for synchronizing the two electrically and mechanically different fly wheel generators and the filter requirements for safe grid synchronization of the dual current direction converters.

Figure 21 shows the allowable apparent power of the EZ3 generator as a function of the effective power supply time. For short pulse duration the supply current is limited by the over current protection system. For a pulse duration beyond 4.5 s the EZ3 supply current is limited by the over temperature protection system. For safe operation there is a sufficient margin required relative to the apparent power boundary of the safety system. As a consequence, the EZ3 supply of apparent power should be kept below about 60 MVA for long pulse operation. This is feasible by means of appropriate reactive power compensation.

7.2 Determination of Required Reactive Power Compensation

To evaluate the accessible long pulse range of ASDEX Upgrade, the following iterative procedure was applied with the goal of completely exhausting the fly wheel energy of the two generators EZ3 and EZ4.

- First, two parameters were assumed and kept constant:
  - the total additional heating power and
  - the plasma flattop time.
- Then, two independent quantities were varied to achieve the desired goal
  - First, the fraction of the total additional heating that can be supplied by the EZ3 generator. The remaining portion of the additional heating was shifted to the EZ4 generator.
  - Then, the flattop loop voltage that can be maintained with the remaining EZ4 fly wheel energy was meximesed.

The result of this procedure is shown in fig. 24 for three levels of the total additional heating power: 10 MW, 15 MW and 20 MW. Due to the limited fly wheel energy the available loop voltage drops with increasing flattop time - the larger the additional heating power, the steeper the decay in loop voltage. For each value of heating power there is a certain flattop loop voltage required (black circles in fig. 24) to maintain the plasma. The black circles in fig. 24 correspond to the lower branch of fig. 9, which represents the ASDEX Upgrade loop voltage condition, found near 10 MW of additional heating. The operational range which can be covered according to fig. 24 comprises a wide range of experimentally highly relevant scenarios.

The shorter the achievable pulse duration of fig. 24, the larger is, for given fly wheel energy, the requirement in apparent power for the EZ3 generator and consequently in reactive power to be compensated. To cover the range of the ASDEX Upgrade additional heating capacity, the reactive power compensation plant has to be dimensioned for $P_{heat} = 20$ MW and a corresponding flattop pulse duration of 9.5 s. Allowing for plasma current ramp-up and ramp-down, this means for the generator EZ3 an effective supply time of 11 s. In table 4 the resulting EZ3 requirements of apparent flattop power are shown for several steps of reactive power compensation. The quoted values are related to the end of flattop, when the frequency has dropped down to 85 Hz. In this case the effective reactive power compensation is only 85% of the nominal value.

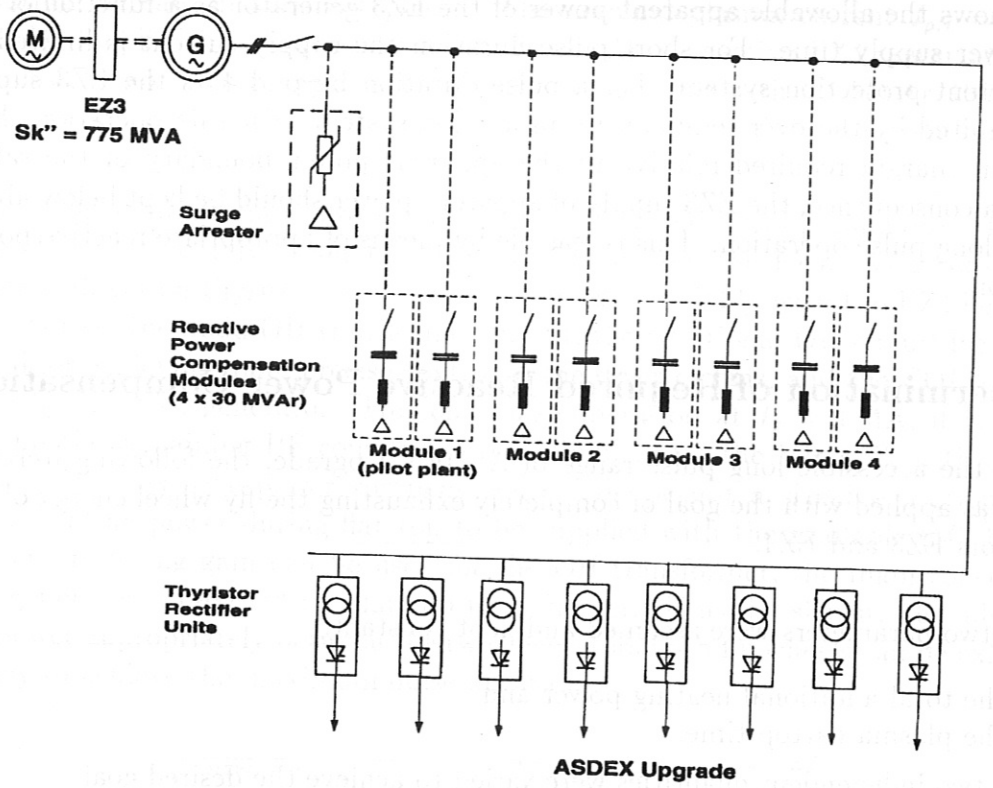

Figure 23: Arrangement of the reactive power compensation modules in ASDEX Upgrade power supply system.

The two points with reactive power compensation are also shown in fig. 21. It is obvious that at nominal 90 MVAr the margin of only 5 MVA (5.5%) to the critical apparent power of 90 MVA, triggering the over temperature safety system, is too small. However, the nominal 120 MVAr compensation is satisfactory. Figure 23 shows schematically the resulting plant, including the generator with voltage protection, the capacitor modules and the thyristor rectifiers supplying ASDEX Upgrade.

For completeness the short pulse values, which result for $I_{pN} = 1.4$ MA, are also quoted. In this case the available apparent power and fly wheel energy of the EZ4 generator are adequate to additionally supply the V1o coil as well. The apparent powers for EZ3 and EZ4 are then

nominal compensated reactive power (MVAr)	effective compensated 85 Hz reactive power (MVAr)	remaining apparent flattop power at 85 Hz (MVAr)	Cos(ϕ) after compensation at 85 Hz
0	0	159	0.2
90	76.5	85	0.37
120	102	62	0.51

Table 4: Power supply conditions of the EZ3 generator after reactive power compensation.

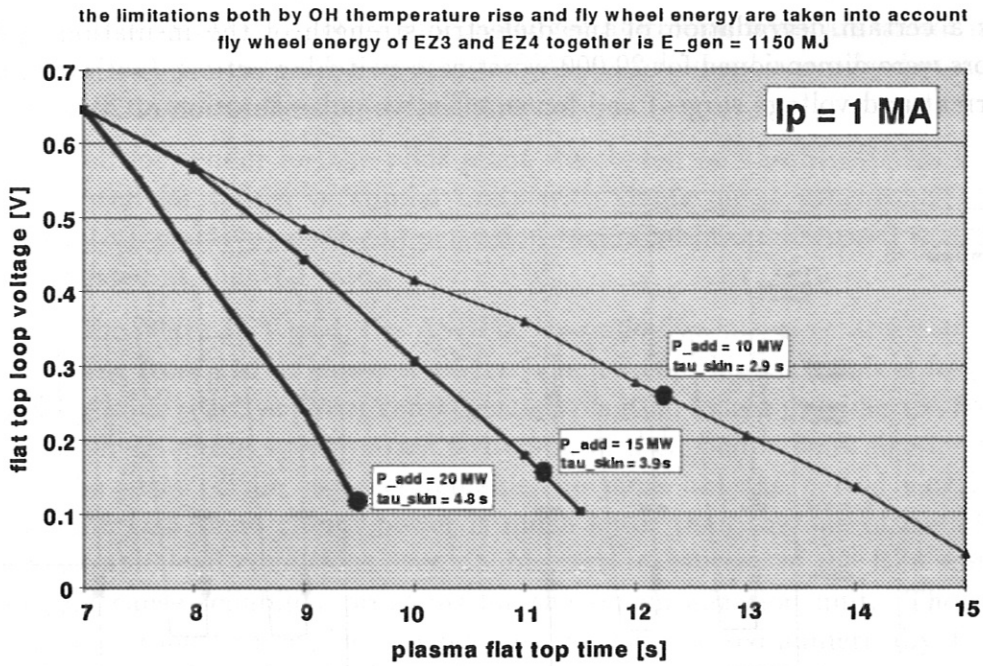

Figure 24: Available loop voltage as a function of the plasma flattop time.

- EZ4: required apparent power 240 MVA. Allowable apparent power 260 MVA
- EZ3: The nominal compensation of 30 MVAr reduces at 85 Hz to 25.5 MVAr. The required apparent power becomes then 127 MVA. The allowable apparent power is 144 MVA.

The pulse duration is limited by the energy supply time over which the nominal apparent power can be provided by the generators. This is, according to fig. 8, about 4.5 s.

7.3 Technical Realization of the Reactive Power Compensation

The considerations which were leading the design of the prototype module 1 are described and extended for the full envisaged plant with 4 modules. Prior to the final specification of the three modules that are the subject of this preferential support application, ample operational experience will be available from running the prototype module 1.

7.3.1 Prototype Capacitor Module 1 for Short Pulse Reactive Power Compensation

The prototype module of fig. 25, consisting of two capacitor units, to be switched on and off by vacuum breakers, were ordered in late 1997 from SIEMENS. Prior to the order SIEMENS was charged with a study contract, which included the general plant layout and numerical computations of the switching surges. As a result of the study contract, the unit size, to be switched as a whole, was chosen to be 15 MVAr/100 Hz in order to keep the voltage surges for the EZ3 stator insulation at a low value. This is mandatory, since the generator EZ3 is now more than 15 years in service. Thus allowance has to

be made for a certain degradation of the dielectric strength of the insulation system. The capacitors were dimensioned for 20.000 worst case switching actions (with maximum transient current and voltage surges) and for an effective pulse duration of 20 s.

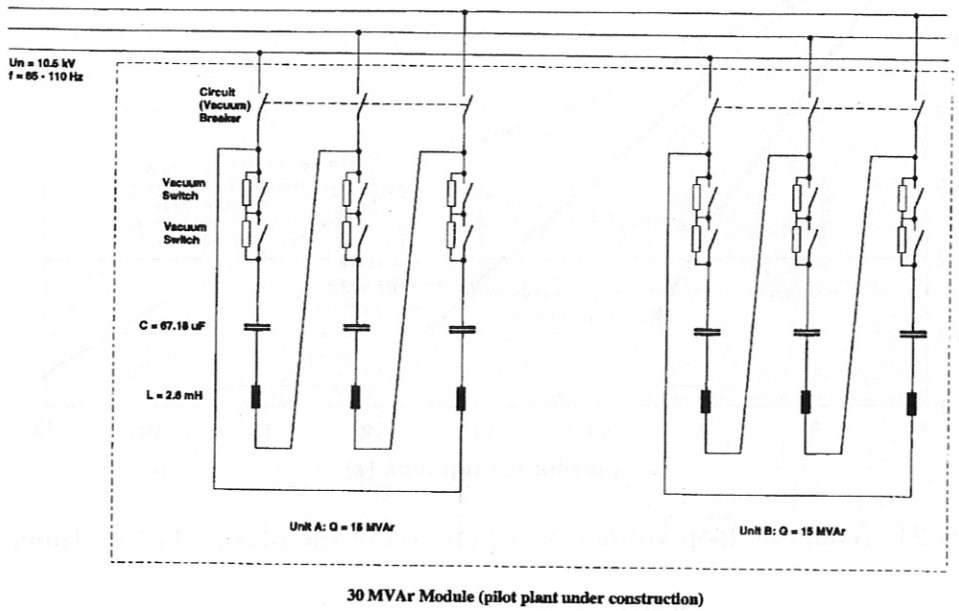

Figure 25: 30 MVAr Module (pilot plant under construction).

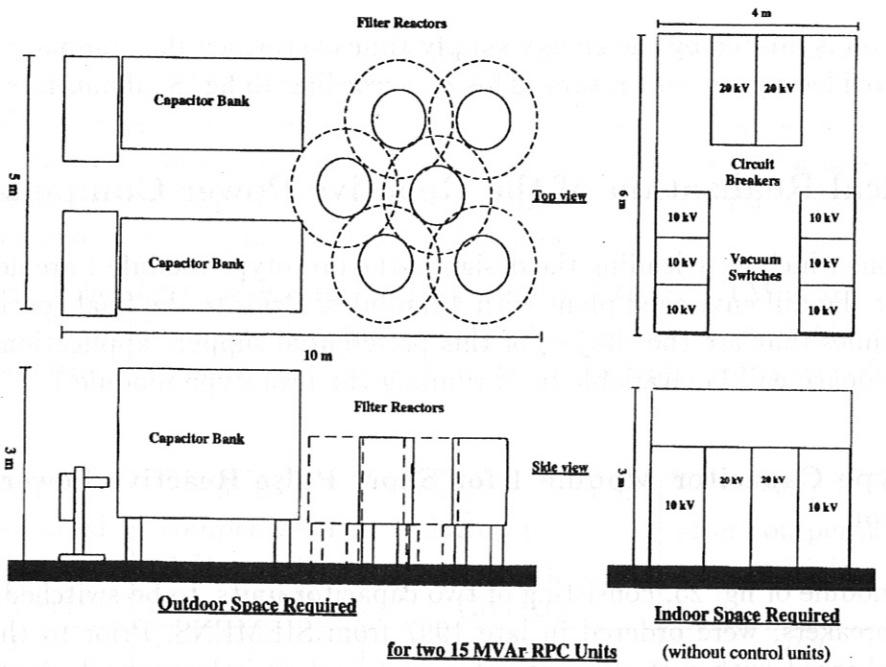

Figure 26: Space requirements of one RPC module.

Figure 25 shows the basic features of a reactive power compensation module and the ratings for the capacitor bank and the filter reactor. The outdoor and indoor space

requirements of the 30 MVAr pilot module, arranged at ground level, are shown in fig. 26. Provisions have been taken that a second 30 MVAr module can be arranged on top of the first one in order to reduce the area requirements.

The ensuing call for tender for the pilot plant was based on the SIEMENS study and a former JET call for tender of similar units with single phase synchronized vacuum switches. The JET reactive power compensation was in addition discussed with the JET team and inspected at the JET site.

In contrast to the 50 Hz JET grid, the ASDEX Upgrade flywheel generators operate at a frequency varying from 110 Hz down to 85 Hz. The twofold higher nominal frequency of the ASDEX Upgrade reactive power compensation plant no longer provides the favourable conditions for single phase synchronized switch-on of a capacitor bank like for the JET plant, since the jitter of the switches remains the same but the period length halves. Furthermore the EZ3 short circuit power is much lower than the one of the JET grid. Under unfavourable load conditions even double zero transitions of the EZ3 voltage can thus occur and cause reliability problems for the synchronization unit. Therefore the surges of the more robust three phase switching were also assessed numerically. Compared to the standard case of synchronized switch-on, only a marginally higher terminal voltage surge resulted; compared to the worst case synchronized switch-on condition, the three phase switching is more favourable.

In order that the three phase circuit breaker of fig. 25 is able to switch-off the capacitor bank, in case the dual vacuum switches are not triggered correctly in one of the three phases due to a problem in the control unit, its nominal voltage was chosen to be as high as 24 kV. Standard switch-off dual switches were chosen for all phases to avoid with certainty any back ignition, since in this case the remaining voltage on the capacitor would increase the terminal voltage of the generator EZ3. The dual switch concept has proven its reliability, switching without fault the resistor for plasma break down almost 10.000 times. Nevertheless, a surge protection will additionally protect the generator EZ3 against re-strike surges. No provisions will be taken for synchronized switch-off of a capacitor bank, since the arc of the vacuum breakers will in any case extinguish only during the zero current crossing.

The combination of the circuit breaker and the single phase dual vacuum switches in fig. 25 permit the realization without change in hardware, of both concepts for switching on a capacitor bank. The control units of module 1 were therefore ordered for both switch-on options. In case the commissioning tests will confirm the computational results for the 3 phase switching, future units will be ordered without synchronized single phase switching. The reason for this is mainly the expected reduction in maintenance and the increase in reliability. The costs saving would only be small.

7.3.2 Plant Description

Characteristics of the Main Plant Components

The 3 phase circuit diagram of the main plant components is shown in Fig. 27. The characteristics of the main plant components are summarized in table 5.

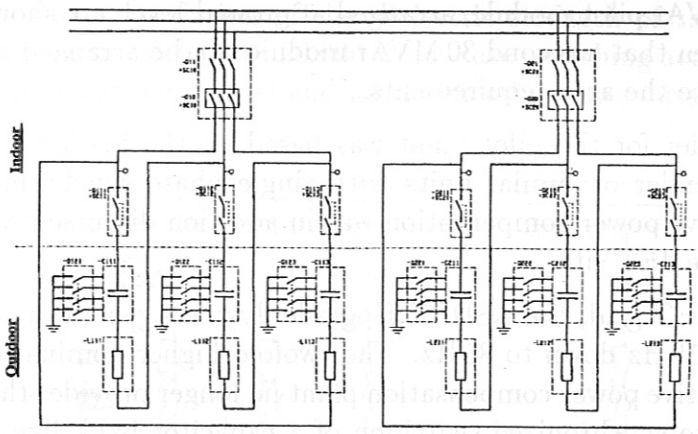

Figure 27: Three phase circuit diagram of main components in each RPC module.

All components will be specified for 20.000 worst case switching actions and must be in accordance with the most recent issues of the relevant IEC standards and recommendations. The control system of the reactive power compensation modules will be integrated into the power supply and ASDEX Upgrade control system as shown in fig. 28.

A Local Control System shall display the status of all control and protective devices of the reactive power compensation system, including auxiliaries. Any switching operations that could endanger parts of the reactive power compensation system or the ASDEX Upgrade power supply system shall be prohibited. Equipment shall automatically enter a safe state in the event of any fault developing in the Programmable Logic Controller (PLC).

The control code of the PLC's for the reactive power compensation units shall be in accordance with the state transition diagram shown in fig. 29. Alarm indications from the reactive power compensation system shall be divided into three groups, each of which shall require different actions to be taken as follows:

- Group A: Emergency shutdown (ESD)
- Group B: Inhibit next pulse (INP)
- Group C: Warning (WG)

The corresponding actions are also shown in that diagram. The following states of the reactive power compensation modules can be defined:

(a) Normal (NL) state
The reactive power compensation module is ready for operation: The circuit breakers are closed, the capacitor bank is discharged, the vacuum double-switches are open and no alarms are sent from group A or B.

(b) Vacuum Switches Enable (VSE) state
The VSE signal is received from the ASDEX Upgrade control system. Reactive power cannot be delivered to the reactive power compensation system outside the VSE window. When under remote control, the VSE signal is generated by the ASDEX Upgrade central timing system.

Circuit Breakers (Q10, Q20)	• three-phase vacuum breakers • $U_N = 24\,\text{kV}$, $I_N = 1250$ A • increased nominal voltage to ensure safe switch-off
Vacuum switches (Q111-Q213)	• single-pole device (two interrupters connected in series as protection against re-striking) • $U_N = 17.5\,\text{kV}$, $I_N = 1250$ A • operating time within $\pm$ 0.5 ms for the guaranteed closing and opening times
Capacitor Banks (C111-C213)	• rated capacitance: 67.18 μ F • $f_N = 85$ Hz - 110 Hz • $U_N = 13.6\,\text{kV}$, • I_N : 600 A, 100 Hz for 20 s and 3 kA, 380 Hz for 200 ms
Filter Reactors (L111-L213)	• rated inductance: 2.57 mH • $f_N = 85$ Hz - 110 Hz • $U_N = 10.5\,\text{kV}$, • I_N : 600A, 100 Hz for 20 s and 3 kA, 380 Hz for 200 ms
Control, Monitoring and Protection	Programmable Logic Controller (PLC) with H1-Bus (Industrial Ethernet) connection for • local and remote control • monitoring • protection • interlocking • alarm handling • signal conditioning • interface to ASDEX Upgrade Control System • operation in feedback control mode or central timing system control mode

Table 5: Characteristics of the main plant components.

(c) Pulse Inhibit (PI) state
The operation of the vacuum double-switches is inhibited. Under normal operation conditions a reactive power compensation unit must enter the Pulse Inhibit state after each pulse because the capacitor bank must be discharged.

(d) Shut Down (SD) state
The circuit breakers of the reactive power compensation unit are open.

(e) Full Down (FD) state
The circuit breakers of the reactive power compensation unit are open and the capacitor short-circuiting/earthing switches are closed.

This is the state in which access is allowed to the high voltage area of the reactive power compensation unit.

(g) Start-Up (STP) transition

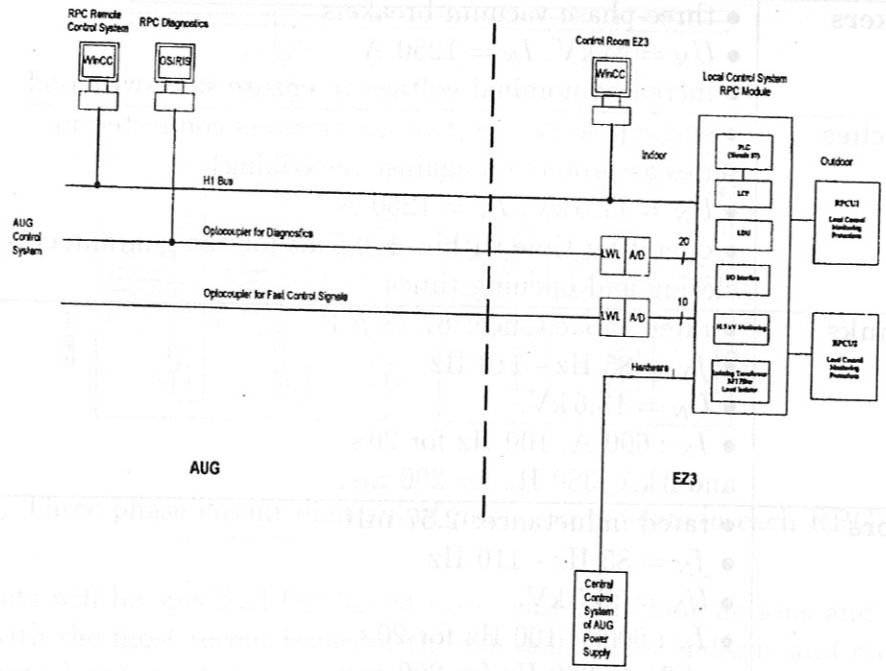

Figure 28: Integration of RPC module into power supply control system.

This transition to the SD state from the FD state is initiated when commands are issued to start the STP sequence shown in fig. 30 (left). These commands can be issued either from the ASDEX Upgrade control system when under remote control, or from the local control panel of the reactive power compensation system when under local control. The transition is completed when the circuit breakers of the reactive power compensation unit are ready for closing.

(h) Pulse Enable (PEN) transition
This transition to the NL state can be initiated from the PI state or from the SD state. The transition is initiated when the command to enable the reactive power compensation system for pulse duty is received either from the ASDEX Upgrade control system or from the local control panel. The transition is completed as soon as the appropriate circuit breakers are closed, the capacitor bank is discharged and no alarms are sent from Unit A or B.

(i) Start of Pulse (SPL) transition
This transition to the VSE state from the NL state is initiated when the VSE signal is issued by the ASDEX Upgrade Control System.

(j) End of Pulse (EPL) transition
This transition to the NL state from the VSE state is initiated when the above VSE signal is removed.

(k) Fast Switch Off (FSO) transition
Under normal operating conditions this transition from the VSE to the PI state must be initiated each time after switch-off of the vacuum switches because the capacitor banks must be discharged before the NL state can be reached.

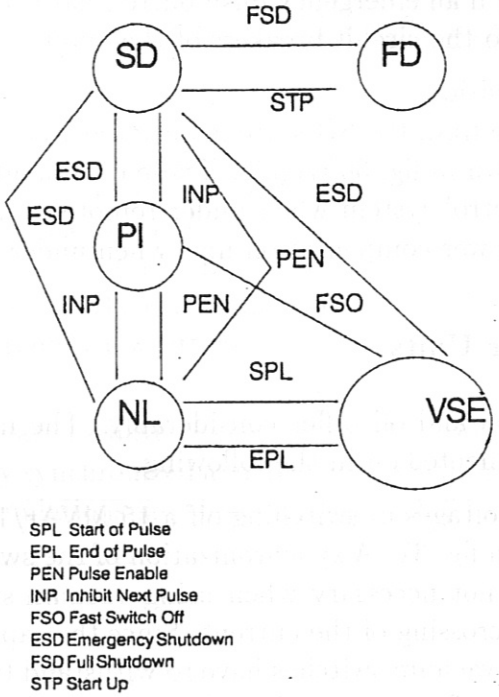

Figure 29: State transition diagram of RPC module control system

(l) Inhibit Next Pulse (INP) transition
This transition to the PI state from the NL state or the SD state is initiated either by Local Unit group B alarms or by a request from the ASDEX Upgrade control system.

(m) Emergency Shutdown (ESD) transition
This transition to the SD state from the NL, PI or VSE states is initiated either by Local Unit group A alarms, by a request from the ASDEX Upgrade control system or by operating an emergency push button. The action of this transition shall be to open

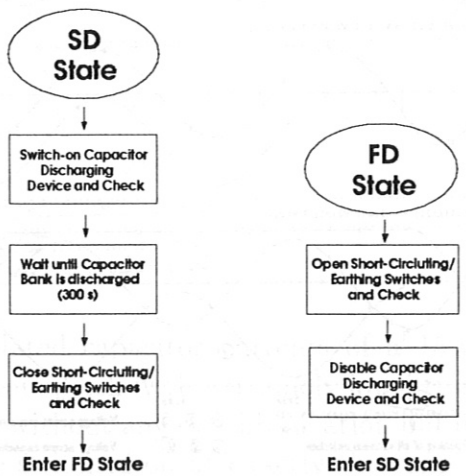

Figure 30: RPC unit full shutdown (left) and start-up (right) sequence.

the vacuum switches of the appropriate reactive power compensation unit (of all reactive power compensation units only if an emergency push button has been operated), and then to issue a tripping command to the circuit breakers of that unit.

(n) Full Shutdown (FSD) transition
This transition to the FD state from the SD state is initiated when commands are issued to start the FSD sequence shown in fig. 30 (right). These commands can be issued either from the ASDEX Upgrade control system when under remote control, or from the local control panel of the reactive power compensation unit when under local control.

Switching off the Capacitor Units

The conditions for switching on and off differ considerably. The main properties of the two switching actions are commented on in the following.

Switching Off: All relevant voltages in switching off a 15 MVAr/100 Hz reactive power compensation unit are shown in fig. 31. A synchronization of the switch-off time with the zero-crossing of the current is not necessary when using vacuum switches because they can only switch-off at the zero crossing of the current. Since the capacitor banks will stay charged after switching off, the vacuum switches have to withstand twice the nominal grid voltage at every regular switch-off operation. In order to have sufficient safety margins, also under fault conditions, the design values shown in fig. 8 and extensive test procedures are stringent and will be laid down in the technical specification of the units.

In order to protect the insulation of the flywheel generator EZ3 against the transient voltage resulting from a restrike after switching off, surge arresters will be provided (fig. 23). These surge arresters shall be of the metal oxide type and shall be installed between the phases of the generator.

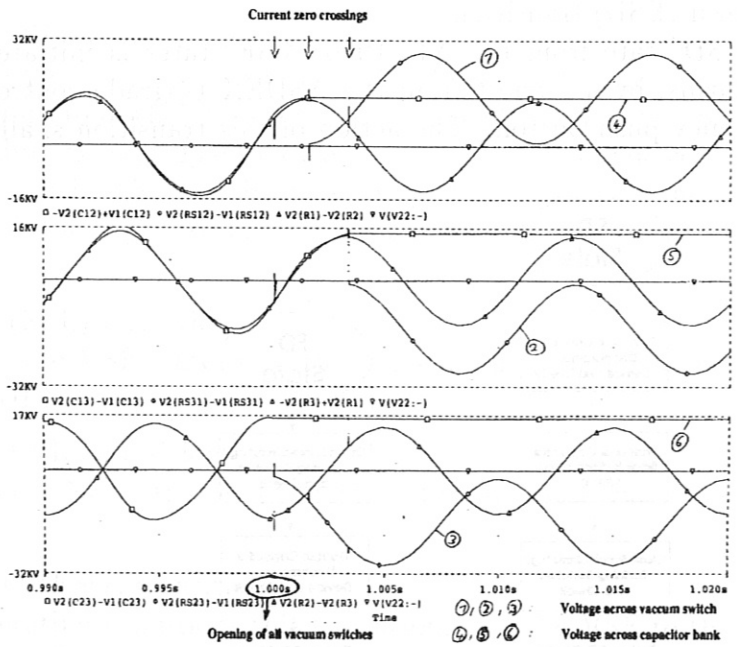

Figure 31: Relevant voltages in switching off a 15 MVAr RPC unit.

Switching On: A synchronization of the switch-on time with the zero-crossing of the voltage will reduce overvoltages and harmonics in the 10.5 kV grid. There are several reasons why a perfect synchronization with the EZ3 grid cannot be realized:

- grid frequency alternating between 85 Hz and 110 Hz,
- sudden load changes occurring during a pulse,
- the load consists of thyristor rectifiers causing a considerable amount of harmonics (difficult recognition of natural current zero),
- weak grid (no connection to the public grid)
- grid frequency up to 110 Hz (problems finding restrike-free high voltage circuit breakers with an extremely low jitter)

Therefore, numerous simulations have been performed in order to investigate the transient effects of not perfectly synchronized and also non-synchronized switch-on operations. Typical results of these simulations are shown in Figs. 32, 33 and 34.

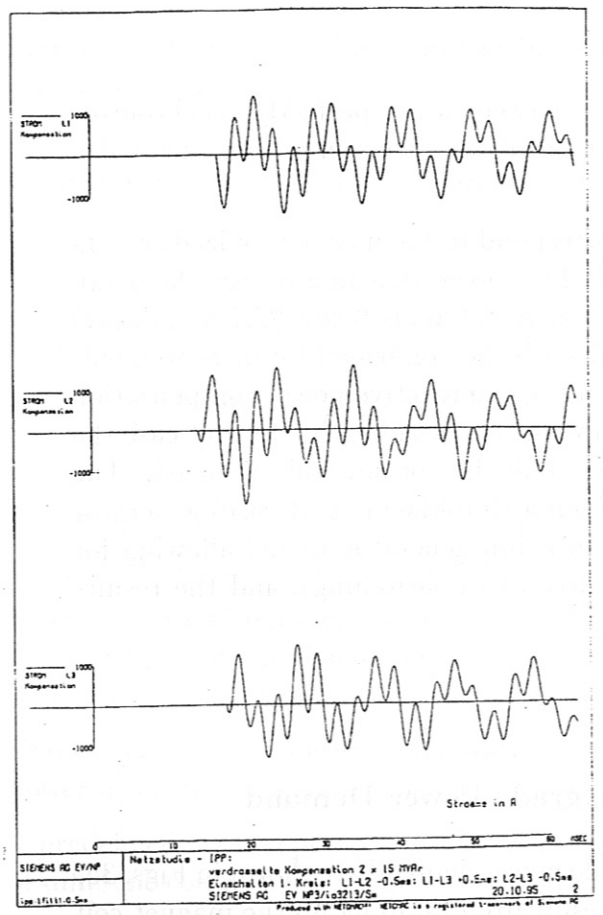

Figure 32: Simulated capacitor currents at synchronized switch-on by Siemens vacuum switches with extremely low jitter (+/- 0.5 ms).

Figure 32 shows the simulated capacitor currents of a 15 MVAr unit when switching on with a SIEMENS vacuum switch with extremely low jitter (± 0.5 ms). The capacitor currents when switching on without any synchronization but using the three-phase circuit breaker (i.e., all phases are switched on at exactly the same time) are shown in fig. 33. The magnitude of the transient capacitor currents is a measure for the transient voltages occurring in the 10.5 kV grid at switch-on. By a comparison of Figs. 32 and 33 it can

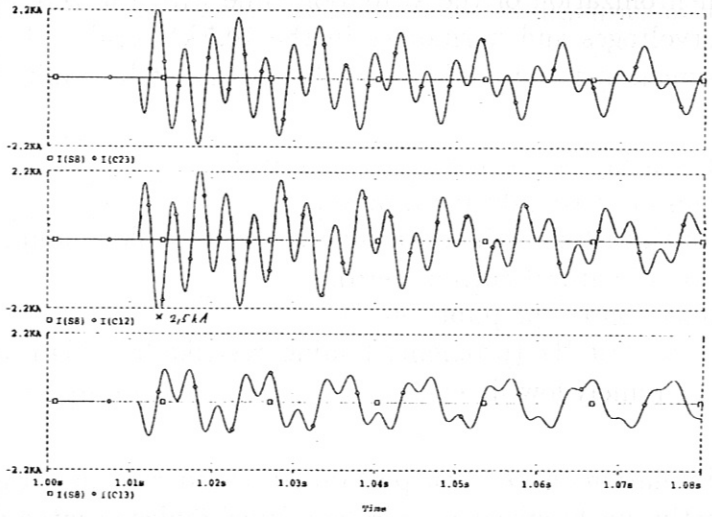

Figure 33: Simulated capacitor currents at unsynchronized switch-on (using the three-phase circuit breakers).

be concluded that there is not much of a difference between a not perfectly synchronized switch-on and a completely unsynchronized switch-on, if the three-phase circuit breaker is used for that switching operation.

The transient voltages in the 10.5 kV grid which correspond to the unsynchronized switch-on (fig. 33) are shown in fig. 34. A parameter study has shown that in any case the maximum transient overvoltage at such an unsynchronized switch-on is below 20% and decays within 50 ms (worst case). If the simulation results will be confirmed by measurements to be performed at the pilot plant (two 15 MVAr units), the reactive power compensation units can be operated without any synchronization with the 10.5 kV grid. In that case the effort for controlling and maintenance of the units could be considerably reduced. The simulation results shown in Figs. 32-34 originate from a simplified (worst case) generator model. Simulations have also been performed with a full generator model allowing for the damper winding of the pole wheel (only for three-phase switching), and the results gained with this model were even more promising.

7.3.3 Plant Operation

Characteristic Time Histories of ASDEX Upgrade Power Demand

Time histories characteristic for the ASDEX Upgrade power demand are shown in Figs. 35, 36 and 37. The first active power peaks in fig. 35 result from ramping up the magnet coil V1u (a poloidal field coil) to an operating current of 30 kA. During the flattop phase of the pulse (11.2 s < t < 15 s in Figs. 35, 36 and 37) this coil current is kept at a constant value leading to a power consumption of 12 MW (ohmic losses). Due to additional heating devices (ICRH) with a power consumption of 14 MW, up to 26 MW are consumed during the flattop phase. Mainly the low power factor of the magnet coil thyristor rectifiers during the flattop phase is the reason for the high reactive power needed by the experiment during that phase of each pulse.

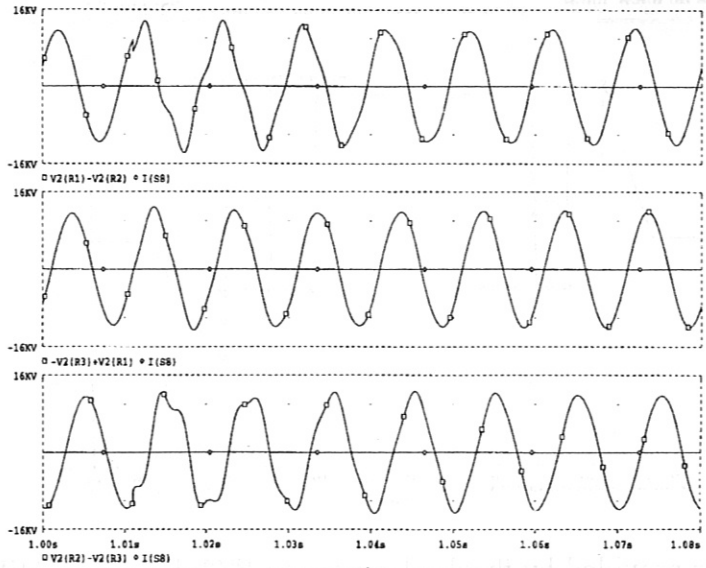

Figure 34: Transient voltages in the 10.5 kV system at unsynchronized switch-on (same simulation as fig. 33).

Reactive Power Compensation System Control Scheme

Each reactive power compensation module can be operated in either:

(a) Feedback control mode, or
(b) Central timing system control mode

When the feedback control mode is enabled, each reactive power compensation unit shall be controlled by the control circuitry associated with measuring the reactive power of the 10.5 kV system.

When the measured reactive power exceeds a predefined level then one reactive power compensation unit shall be switched on. That power level shall be adjustable.

If the first reactive power compensation unit is already switched on and a predefined (adjustable) level of reactive power is exceeded, then the second reactive power compensation unit shall be switched on.

The second reactive power compensation unit shall be switched off if the measured reactive power drops under a predefined (adjustable) level.

A predefined waiting period T_{diff}(0–500 ms) shall be kept between the switching processes of different compensation units.

In case of malfunction of the first reactive power compensation unit, the second reactive power compensation unit shall be switched on if the measured reactive power exceeds a predefined (adjustable) level after the waiting period T_{diff} and after it has been detected that the first reactive power compensation unit is still switched off.

If the feedback control mode is disabled, each reactive power compensation unit shall be controlled by ASDEX Upgrade central timing system commands.

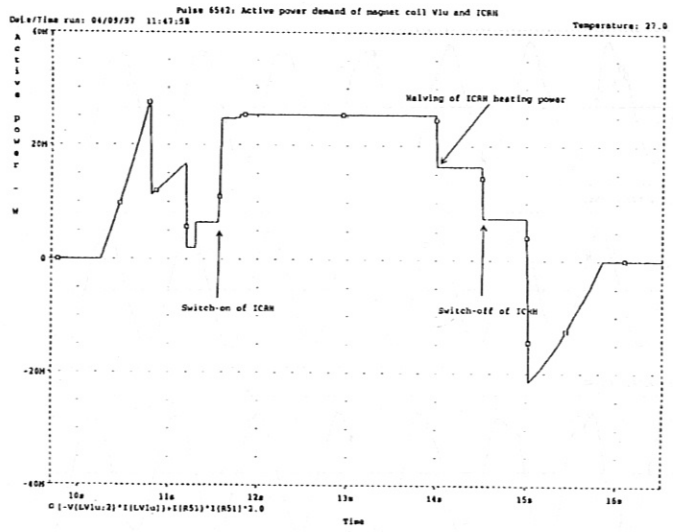

Figure 35: Active power provided by flywheel generator EZ3 during an ASDEX Upgrade pulse (one magnet coil and devices for plasma heating being supplied by flywheel generator EZ3).

After a reactive power compensation unit has been switched off, it shall not be switched on again before the next nominal pulse. This is to ensure that the residual voltage of the capacitor banks has decreased sufficiently before re-energizing.

Main Fault Conditions of Reactive Power Compensation System

- Over current

Should an over current develop within any reactive power compensation unit, it shall be detected by means of an over current monitoring device, a group A alarm shall be issued and an Emergency Shutdown (ESD) of the appropriate reactive power compensation unit shall be performed.

The operating level of the above device shall be properly co-ordinated with those of the overcurrent relays of the 10.5 kV distribution system.

- Prolonged Operation

Should current continue to flow in a reactive power compensation unit for a period longer than 20 s, it shall be detected by means of an appropriate current monitoring device. The protective action shall be to issue a group A alarm and to perform an Emergency Shutdown (ESD) of the appropriate reactive power compensation unit.

- Excess Leakage current

Should the leakage current in any single-phase element of a reactive power compensation unit exceed a predetermined maximum level, it shall be detected by means of an overcurrent monitoring device. The protective action shall be to issue a group A alarm and to perform an Emergency Shutdown (ESD) of the appropriate reactive power compensation unit.

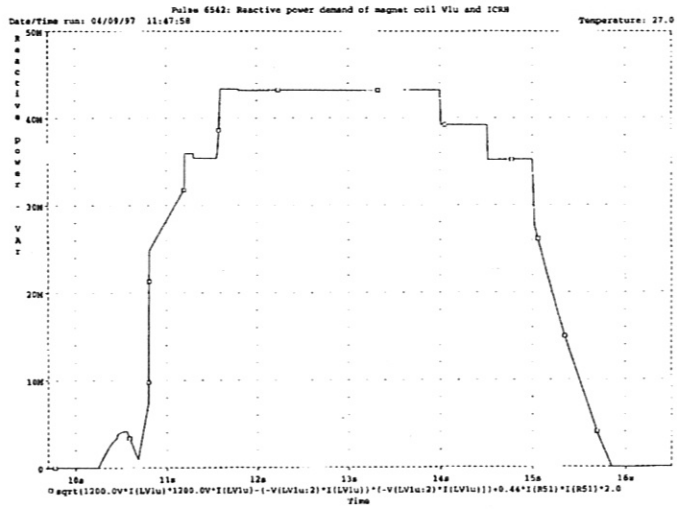

Figure 36: Reactive power provided by flywheel generator EZ3 during an ASDEX Upgrade pulse (one magnet coil and devices for plasma heating being supplied by flywheel generator EZ3).

- Vacuum Switch Closing Failure

Vacuum Switch closing failure can occur in the following ways:

- Failure to Close: i.e., when a closing command is issued to a Vacuum Switch and no "closed" indication is received from that switch within a specified time period.
- Self Closing: i.e., when a "closed" indication is received from a Vacuum Switch and no closing command has been issued to that switch .

Should a Vacuum Switch closing failure occur in one or more phases, it shall be detected by means of an appropriate monitoring device. The protective action shall be to issue a group A alarm and to perform an Emergency Shutdown (ESD) of the appropriate reactive power compensation unit.

- Capacitor Breakdown

Should capacitor breakdown occur during a Nominal Pulse, it shall be detected by monitoring the resulting imbalance current. The protective action shall be to issue a group A alarm and to perform an Emergency Shutdown (ESD) of the appropriate reactive power compensation unit.

Capacitor breakdown occurring outside a Nominal Pulse, shall be detected by a method to be determined with the Supplier. The protective action shall be to issue a group B alarm and to Inhibit the Next Pulse (INP) for the faulty reactive power compensation unit.

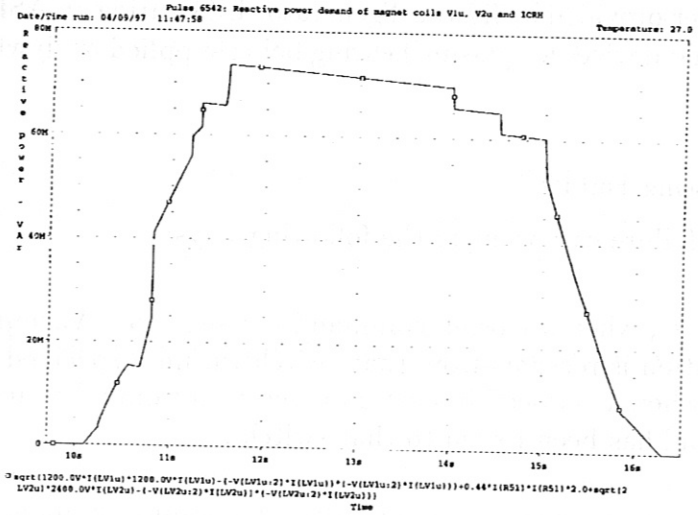

Figure 37: Reactive power provided by flywheel generator EZ3 during an ASDEX Upgrade pulse (two magnet coils and devices for plasma heating being supplied by flywheel generator EZ3).